

# Fixed-Time Adaptive Consensus Control for Multi-Quadrotor Subject to External Disturbances Via Deep Reinforcement Learning

Yefeng Yang, Kang Liu, Li-Yu Lo, Tao Huang, Yanming Fu, Chih-Yung Wen

**Abstract**—This paper addresses a fully distributed consensus control problem for multi-quadrotor formation control. First, a type of fully distributed fast nonsingular terminal sliding mode controller (FNTSMC) is introduced for both the rotational and translational subsystems. To accurately estimate external disturbances, a fixed-time disturbance observer is implemented, where the estimation error converges to the vicinity of the origin within a fixed time. Additionally, a deep reinforcement learning-based optimizer is incorporated into the FNTSMC to adaptively tune its hyperparameters, enhancing the quadrotors' flight performance. The entire system is proven to be fixed-time stable in the Lyapunov sense. Finally, extensive numerical simulations and physical experiments are conducted to verify the effectiveness and superiority of the proposed control framework.

**Note to Practitioners**—In recent years, artificial intelligence has increasingly influenced traditional control systems. This paper focuses on developing a unified control framework that integrates fast nonsingular terminal sliding mode controllers (FNTSMCs) with deep reinforcement learning (DRL) techniques. The primary motivation for designing this hybrid framework arises from the impact of parameter tuning on control performance in traditional control systems, especially in real-world scenarios. Initially, FNTSMCs and fixed-time disturbance observers were developed for quadrotor groups to ensure fixed-time stability in the Lyapunov sense. However, manual tuning of hyperparameters in FNTSMCs is challenging, and real-time adjustments are required to adapt to varying conditions. Therefore, to enhance control performance, DRL is employed as an optimization framework to learn an adaptive, neural network-based tuning law for the FNTSMC. Extensive numerical simulations and physical experiments confirm the effectiveness and superiority of the proposed framework. Future research will focus on online distributed parameter optimization using DRL, as well as multi-quadrotor consensus control involving switching topologies and communication delays.

**Index Terms**—Quadrotor consensus control, fixed-time control, deep reinforcement learning control, disturbance observer, sliding mode control.

## I. INTRODUCTION

This work is supported by the Research Center of Unmanned Autonomous Systems (RCUAS), The Hong Kong Polytechnic University under Grant P0046487.

Yefeng Yang, Kang Liu, Li-Yu Lo, Tao Huang, and Chih-Yung Wen are with the Department of Aeronautical and Aviation Engineering, The Hong Kong Polytechnic University, Hong Kong, China(e-mail: yefeng.yang@connect.polyu.hk, k\_liu@ieee.org, patty.lo@connect.polyu.hk, tao755.huang@connect.polyu.hk, cywen@polyu.edu.hk).

Yefeng Yang, Tao Huang, and Yanming Fu are with the Center for Control Theory and Guidance Technology, Harbin Institute of Technology(e-mail: yefeng.yang@connect.polyu.hk, tao755.huang@connect.polyu.hk, fuyanming@hit.edu.cn).

In recent years, quadrotor technology has made significant advancements across various industrial applications such as surveillance [1], search and rescue operations [2], environmental monitoring [3], and delivery services [4]. However, given that some tasks involve wide spatial distribution, complex task composition, and extended time requirements, a single quadrotor often struggles to complete such missions independently. As a result, cooperative control of multiple quadrotors has become a prevailing trend in the field. Coordinating multiple quadrotors presents unique challenges beyond those encountered in single-quadrotor control, including collision avoidance, flight formation maintenance, and synchronized movements, all of which require advanced algorithms and robust communication systems. On the other hand, the potential benefits of multi-quadrotor systems include enhanced efficiency, greater coverage, and the capability to perform complex tasks that a single quadrotor cannot accomplish alone. Consequently, research in multi-quadrotor control is essential for advancing the capabilities and applications of quadrotors.

Although multi-quadrotor control has broad application prospects, it still faces numerous challenges compared to single-quadrotor control. To address the consensus control of multi-quadrotor formations, many researchers have presented robust solutions. For example, a distributed adaptive leader-follower control protocol for a class of strict-feedback nonlinear systems was proposed in [5]. Considering convergence time, an adaptive finite-time control protocol for nonlinear multi-agent systems was introduced in [6]. A finite-time leader-follower consensus controller based on backstepping theory, which compensates for mismatched disturbances, was presented in [7]. Although the methods proposed in previous works are finite-time stable, the convergence time cannot be estimated. Therefore, many fixed-time control methods are introduced. Zhao et al. [8] introduced an fixed-time event-triggered sliding mode controller (SMC) for multi-agent consensus control problems with unknown dynamics. Khodaverdian et al. [9] proposed a predictor-based fixed-time SMC for multi-quadrotor systems. However, they required that the estimation of the unknown part of the system to be bounded. Miao et al. [10] proposed a fixed-time fault-tolerant controller for multi-quadrotor systems. Nevertheless, the proposed method required the disturbances and their derivatives are all bounded. To solve these problems, this study aims to design a feasible fixed-time formation controller for multi-quadrotor with unknown disturbances to improve system robustness.

Among the controllers mentioned above, the sliding mode-

based control framework stands out for its robustness, fast response, and simple design. Liang et al. [11] introduced a multi-aircraft aerial transportation framework by combining backstepping and sliding mode control (SMC). Hou et al. [12] proposed an adaptive sliding mode-based method for multi-quadrrotor trajectory tracking control under environmental uncertainties. Liang et al. [13] extended the application of quadrotors by adding a robotic manipulator and proposing an adaptive prescribed performance controller for the system. In [14], Ijaz et al. developed an integral sliding mode-based control scheme with a novel fault estimation mechanism for quadrotor systems. Although sliding mode controllers (SMCs) offer significant advantages and have been extensively studied, parameter tuning in SMCs remains a challenging issue. If the gain of an SMC is set too high, it may cause overshoot and chattering; conversely, insufficient gain can slow the convergence of the sliding variables. Therefore, developing a time-varying adaptive tuning law is essential for improving the practical implementation of multi-quadrrotor systems.

Deep reinforcement learning (DRL) is well-suited for complex function approximation and is naturally applicable to parameter optimization. In fact, DRL has already been combined with some traditional controllers. In [15], approximate dynamic programming (ADP), a DRL technique from the control theory perspective, was integrated with sliding mode control (SMC) to manage multi-agent systems. However, this approach decoupled the ADP learning process from the sliding mode surface design, effectively using pure ADP control rather than SMC as the actual controller. Mousavi et al. [16] proposed a multi-agent consensus control framework that combines fuzzy control, SMC, and DRL, utilizing fuzzy-based DRL to optimize the sliding mode surface. However, similar to the previous approach, the final controllers relied on a pure neural network (NN) rather than a hybrid of NN and traditional methods. Although ultimately uniformly bounded stability can be proven, the performance of the tuning process before NN weights are fully converged cannot be guaranteed. Additionally, the so-called boundary of the tracking error in pure NN-based control cannot be analytically formulated. Therefore, rather than directly learning the complex nonlinear mapping between states and actuators, using DRL to optimize specific hyperparameters of controllers is a more favorable choice.

Based on the preceding analysis and summary, the main contributions of this study are as follows:

- 1) A fully distributed fast nonsingular terminal sliding mode controller (FNTSMC) is proposed to address the multi-quadrrotor consensus control problem, ensuring fixed-time stability in the Lyapunov sense. Compared to the works presented in [5]–[7], the proposed FNTSMC enables the quadrotors to accurately track reference trajectories while maintaining formation within a fixed time.
- 2) A fixed-time disturbance observer (FTDO) is introduced to estimate unknown external disturbances, where the estimation error converges to a neighborhood of the origin within a fixed time. Unlike the observers proposed in [17], [18], this observer does not require the disturbances to vary slowly enough for their time derivatives to be approximately zero.

3) In contrast to the methods proposed in [19]–[22], the deep reinforcement learning (DRL) technique is utilized to optimize the hyperparameters of the fast nonsingular terminal sliding mode controllers (FNTSMCs), rather than directly replacing the controller with a single-layer linear neural network approximator. The combination of DRL and FNTSMC not only ensures that the fixed-time stability of the system remains intact, but also enhances the robustness and flight performance of the quadrotor formation. Finally, extensive simulations and physical experiments are conducted to verify the effectiveness and superiority of the proposed control framework.

The remainder of the paper is organized as follows: Section II introduces some preliminaries and outlines the problem addressed in this study. The controller design is presented in Section III. In Section IV, a reinforcement learning-based parameter optimization framework is introduced to further improve the hyperparameters of the FNTSMCs. Simulations and experiments are conducted in Section V and Section VI, respectively. Finally, Section VII concludes the paper.

*Notations:* In what follows,  $\text{diag}(\cdot)$  denotes the diagonal matrix, and  $\circ$  represents the Hadamard product operator.  $C_{(\cdot)}$ ,  $S_{(\cdot)}$ , and  $T_{(\cdot)}$  denote the cosine, sine, and tangent functions, respectively. For a vector  $x \in \mathbb{R}^n$ ,  $|x| = [|x_1|, |x_2|, \dots, |x_n|]^T$ , and  $[x]^\alpha = |x|^\alpha \circ \text{sgn}(x)$ . The vector  $\eta = [x, y, z]^T$  represents the position of the quadrotor,  $\rho = [\phi, \theta, \psi]^T$  denotes the attitude of the quadrotor, and  $\omega = [p, q, r]^T$  is the angular rate. The parameters  $k_t$  and  $k_r$  represent the translational and rotational drag coefficients, respectively. The inertia tensor matrix of the quadrotor is given by  $J = \text{diag}(J_{xx}, J_{yy}, J_{zz})$ . The symbol  $g$  denotes the gravitational acceleration,  $\tau = [\tau_x, \tau_y, \tau_z]^T$  represents the torque, and  $u_f$  is the throttle.

## II. PRELIMINARIES AND PROBLEM FORMATION

### A. Fundamental Mathematics

The entire quadrotor group consisting of  $N$  quadrotors can be abstracted as a graph  $\mathcal{G} = (\mathcal{V}, \mathcal{E})$ . The set of nodes  $\mathcal{V} = \{v_1, v_2, \dots, v_N\}$  represents each quadrotor. The set of edges  $\mathcal{E} = \{(v_i, v_j)\}$  denotes the connections in  $\mathcal{G}$ , with  $(v_i, v_j)$  representing the edge between  $v_i$  and  $v_j$ . The existence of the edge  $(v_i, v_j)$  indicates that information can be transmitted from  $v_i$  to  $v_j$ . The neighbor set of  $v_i$  is defined as  $\mathcal{N}_i = \{v_j | (v_j, v_i) \in \mathcal{E}\}$  if the edge  $(v_j, v_i)$  exists. Correspondingly, the adjacency matrix is denoted by  $\mathcal{A} = [a_{ij}] \in \mathbb{R}^{N \times N}$  with weights  $a_{ij} = 1$  if  $(v_j, v_i) \in \mathcal{E}$  and  $a_{ij} = 0$  if  $(v_j, v_i) \notin \mathcal{E}$ . Specifically, the graph is undirected if  $a_{ij} = a_{ji}, \forall i, j = 1, 2, \dots, N$ , and the graph is directed if there exists at least one tuple  $(i, j)$  such that  $a_{ij} \neq a_{ji}$ . The in-degree matrix of  $\mathcal{G}$  is defined as  $\mathcal{D} = \text{diag}(d_1, d_2, \dots, d_N)$  with  $d_i = \sum_{j=1}^N a_{ji}, i = 1, 2, \dots, N$ . The Laplacian matrix of the graph  $\mathcal{G}$  is defined as  $\mathcal{L} = [l_{ij}] \in \mathbb{R}^{N \times N} = \mathcal{D} - \mathcal{A}$ . For leader-follower control problems, the leader adjacency matrix (or communication matrix) is described as  $\mathcal{B} = \text{diag}(b_i), i = 1, 2, \dots, N$ , where  $b_i = 1$  if and only if  $v_i$  can receive information from the leader node; otherwise,  $b_i = 0$ . The augmented graph, which includes the leader node  $v_b$ , is

denoted as  $\mathcal{G}_B = (\mathcal{V}, \mathcal{E}, v_b, b_i)$ ,  $i = 1, 2, \dots, N$ . Without loss of generality, we make the following assumption.

*Assumption 1.* For the graph theory used in the study, the following standard conditions are required:

- 1) Like in [23], the graph  $\mathcal{G}$  is undirected.
- 2) Similar to [24], there are no self-loops in the graph  $\mathcal{G}$ . Namely,  $a_{ii} = 0$ ,  $i = 1, 2, \dots, N$ .
- 3) There exists at least one spanning tree with the leader node  $v_b$  as the root of graph  $\mathcal{G}_B$  [24].

*Assumption 2.* [25] The disturbances  $\Delta_{\rho,i}$ ,  $\Delta_{\eta,i}$  acted on the  $N$  quadrotors are bounded by unknown positive constants, namely,  $\|\Delta_{\rho,i}\| \leq \bar{\delta}$  and  $\|\Delta_{\eta,i}\| \leq \bar{\Delta}$ .

*Assumption 3.* [26] The yaw angle is bounded as  $\psi_i \in [-\pi, \pi]$ . To avoid singularities, the pitch and roll angles are bounded as  $\phi_i, \theta_1 \in (-\frac{\pi}{2}, \frac{\pi}{2})$ .

For clarity and convenience, some useful lemmas are listed as follows.

*Lemma 1.* [27] For undirected graph, the matrix  $\mathcal{H} = \mathcal{L} + \mathcal{B}$  is symmetrical positive definite if the graph  $\mathcal{G}$  is connected and at least one follower can receive the leader's information.

*Lemma 2.* [28] For system  $\dot{x} = f(x)$ ,  $f(0) = 0$ , where  $x \in \mathbb{R}^n$  is the state and  $f(x) \in \mathbb{R}^n$  is the system dynamics. If there exists a continuous function  $V(x)$  such that

$$\dot{V}(x) \leq -[a_1 V(x)^{m_1} + a_2 V(x)^{m_2}]^k,$$

where  $a_1 > 0$ ,  $a_2 > 0$ ,  $m_1 > 0$ ,  $m_2 > 0$ ,  $k > 0$ ,  $km_1 < 1$ , and  $km_2 > 1$ . Then, the origin of the system is fixed-time stable, and the settling time  $T$  is bounded by

$$T \leq T_{max} = \frac{1}{a_1^k (1 - km_1)} + \frac{1}{a_2^k (km_2 - 1)}.$$

*Lemma 3.* [29]  $\forall x_i \in \mathbb{R}$ ,  $i = 1, 2, \dots, n$ ,  $0 < p \leq 1$ , there is

$$\left( \sum_{i=1}^n |x_i| \right)^p \leq \sum_{i=1}^n |x_i|^p \leq n^{1-p} \left( \sum_{i=1}^n |x_i| \right)^p.$$

*Lemma 4.* [30]  $\forall x, y \in \mathbb{R}$  and  $v > 1$ , there is  $|x + y|^v \leq 2^{v-1} |x^v + y^v|$ .

## B. System Description

According to [31], the dynamic of the  $i$ -th quadrotor can be described as

$$\begin{aligned} \ddot{\eta}_i &= \frac{u_{f,i}}{m_i} A_i(\rho_i) - \mathbf{g} - \frac{k_t}{m_i} \dot{\eta}_i + \frac{\delta_{\eta,i}}{m_i}, \\ \dot{\omega}_i &= J^{-1} [-k_r \omega_i - \omega_i \times (J\omega) + \delta_{\rho,i} + \tau_i], \\ \dot{\rho}_i &= W_i(\rho_i) \omega_i, \end{aligned} \quad (1)$$

where  $\eta_i$ ,  $u_{f,i}$ ,  $k_t$ , and  $m_i$  respectively represents the position, throttle, drag coefficient of the translational loop, and mass of the  $i$ -th quadrotor,  $\mathbf{g} = [0, 0, g]^T$  is the gravity,  $\delta_{\eta,i}$  is the external disturbance of the translational loop;  $\omega_i$ ,  $J$ ,  $k_r$ , and  $\tau_i$  respectively denotes the angular rate, inertia tensor matrix, drag coefficient of the rotational loop, and torque of the  $i$ -th

quadrotor; and  $A_i \triangleq A_i(\rho_i)$  and  $W_i \triangleq W_i(\rho_i)$  are respectively defined as [32]

$$\begin{bmatrix} C_{\varphi,i} C_{\psi,i} S_{\theta,i} + S_{\varphi,i} S_{\psi,i} \\ C_{\varphi,i} S_{\psi,i} S_{\theta,i} - S_{\varphi,i} C_{\psi,i} \\ C_{\theta,i} C_{\varphi,i} \end{bmatrix}, \begin{bmatrix} 1 & S_{\varphi,i} T_{\theta,i} & C_{\varphi,i} T_{\theta,i} \\ 0 & C_{\varphi,i} & -S_{\varphi,i} \\ 0 & S_{\varphi,i}/C_{\theta,i} & C_{\varphi,i}/C_{\theta,i} \end{bmatrix},$$

and  $\delta_{\eta,i}$  and  $\delta_{\rho,i}$  respectively denote the disturbances acted on rotational and translational subsystems of the  $i$ -th quadrotor.

1) *Rotational Subsystem:* The tracking error  $e_{\rho,i}$  and the 1<sup>st</sup> and 2<sup>nd</sup> order derivatives of  $e_{\rho,i}$  are given by

$$\begin{aligned} e_{\rho,i} &= \rho_i - \rho_{d,i} \\ \dot{e}_{\rho,i} &= W_i \omega_i - \dot{\rho}_{d,i}, \\ \ddot{e}_{\rho,i} &= \dot{W}_i \omega_i + W_i \dot{\omega}_i - \ddot{\rho}_{d,i}, \end{aligned} \quad (2)$$

where  $\rho_{d,i} = [\phi_{d,i}, \theta_{d,i}, \psi_{d,i}]^T$  is the reference attitude angle, and

$$\dot{W}_i = \begin{bmatrix} 0 & \dot{\varphi}_i T_{\theta,i} C_{\varphi,i} + \frac{\dot{\theta}_i S_{\varphi,i}}{C_{\theta,i}^2} & -\dot{\varphi}_i S_{\varphi,i} T_{\theta,i} + \frac{\dot{\theta}_i C_{\varphi,i}}{C_{\theta,i}^2} \\ 0 & -\dot{\varphi}_i S_{\varphi,i} & -\dot{\varphi}_i C_{\varphi,i} \\ 0 & \frac{\dot{\varphi}_i C_{\varphi,i} C_{\theta,i} + \dot{\theta}_i S_{\varphi,i} S_{\theta,i}}{C_{\theta,i}^2} & -\dot{\varphi}_i S_{\varphi,i} C_{\theta,i} + \dot{\theta}_i C_{\varphi,i} S_{\theta,i} \end{bmatrix}.$$

By defining  $\Delta_{\rho,i} = J_i^{-1} \delta_{\rho,i} - \ddot{\rho}_{d,i}$ ,  $f_{\rho,i} = -J_i^{-1} [k_r \omega_i + \omega_i \times (J_i \omega_i)]$ ,  $A_{\rho,i} = \dot{W}_i \omega_i + W_i f_{\rho,i}$ ,  $B_{\rho,i} = W_i J_i^{-1}$  and doing some manipulations, Eq. (2) can be finally simplified as

$$\ddot{e}_{\rho,i} = A_{\rho,i} + B_{\rho,i} \tau_i + \Delta_{\rho,i}. \quad (3)$$

*Remark 1.* Note that the second-order derivative of  $\rho_{d,i}$  is known for pure attitude control. However, in the case of position control, the desired attitude commands are generated by the translational subsystem. As a result,  $\ddot{\rho}_{d,i}$  is absorbed into  $\Delta_{\rho,i}$  and treated as part of the unknown disturbances.

2) *Translational Subsystem:* The virtual expected acceleration of the  $i$ -th quadrotor can be defined as

$$u_{\eta,i} = [a_{x,i}, a_{y,i}, a_{z,i}]^T, \quad (4)$$

yielding

$$\ddot{\eta}_i = -\frac{k_t}{m_i} \dot{\eta}_i + u_{\eta,i} + \Delta_{\eta,i}, \quad (5)$$

where  $\Delta_{\eta,i} = \frac{u_{f,i}}{m_i} A_i + \frac{\delta_{\eta,i}}{m_i} - \mathbf{g} - u_{\eta,i}$  is the equivalent disturbance. Thereafter, it can be easily derived that

$$\begin{aligned} u_{f,i} &= m_i \sqrt{a_{x,i}^2 + a_{y,i}^2 + (a_{z,i} + g)^2} \\ \varphi_{d,i} &= \arcsin \frac{m_i [a_{x,i} S_{\psi,i} - a_{y,i} C_{\psi,i}]}{u_{f,i}} \\ \theta_{d,i} &= \arctan \frac{a_{x,i} C_{\psi,i} + a_{y,i} S_{\psi,i}}{a_{z,i} + g}. \end{aligned} \quad (6)$$

Based on the derivation above, the consensus tracking error of the  $i$ -th quadrotor can be defined as

$$e_{\eta,i} = \sum_{j=1}^N a_{ij} [(\eta_j - \nu_j) - (\eta_i - \nu_i)] + b_i (\eta_i - \eta_d - \nu_i), \quad (7)$$

where  $\eta_d$  is the reference geometric center of the quadrotor formation and  $\nu_i$  is the offset of the  $i$ -th quadrotor to the geometric center.

For ease of theoretical derivation, a new variable can be defined as

$$\Lambda_i = b_i \eta_d + (b_i + d_i) \nu_i + \sum_{j=1}^N a_{ij} (\eta_j - \nu_j). \quad (8)$$

Correspondingly, one obtains

$$\begin{aligned} \dot{\Lambda}_i &= b_i \dot{\eta}_d + (b_i + d_i) \dot{\nu}_i + \sum_{j=1}^N a_{ij} (\dot{\eta}_j - \dot{\nu}_j), \\ \ddot{\Lambda}_i &= b_i \ddot{\eta}_d + (b_i + d_i) \ddot{\nu}_i + \sum_{j=1}^N a_{ij} (\ddot{\eta}_j - \ddot{\nu}_j). \end{aligned} \quad (9)$$

Further, substituting  $\ddot{\eta}_j$  into  $\ddot{\Lambda}_i$  and doing some manipulations yield

$$\begin{aligned} \ddot{\Lambda}_i &= b_i \ddot{\eta}_d + (b_i + d_i) \ddot{\nu}_i + \sum_{j=1}^N a_{ij} (\ddot{\eta}_j - \ddot{\nu}_j) \\ &= b_i \ddot{\eta}_d + (b_i + d_i) \ddot{\nu}_i \\ &\quad + \sum_{j=1}^N a_{ij} \left( -\frac{k_{t,j}}{m_j} \dot{\eta}_j + u_{\eta,j} + \Delta_{\eta,j} - \ddot{\nu}_j \right) \\ &= \Lambda_{i0} + \sum_{j=1}^N a_{ij} \Delta_{\eta,j}, \end{aligned} \quad (10)$$

where  $\Lambda_{i0} = b_i \ddot{\eta}_d + (b_i + d_i) \ddot{\nu}_i + \sum_{j=1}^N a_{ij} \left( -\frac{k_{t,j}}{m_j} \dot{\eta}_j + u_{\eta,j} + \Delta_{\eta,j} - \ddot{\nu}_j \right)$  is a known variable. Then, the error dynamics of the translational loop can be given by

$$\begin{aligned} \ddot{e}_{\eta,i} &= -\frac{(d_i + b_i) k_{t,i}}{m_i} \dot{\eta}_i + (b_i + d_i) u_{\eta,i} - \Lambda_{i0} \\ &\quad + (b_i + d_i) \Delta_{\eta,i} - \sum_{j=1}^N a_{ij} \Delta_{\eta,j}. \end{aligned} \quad (11)$$

### C. Problem Formation

Based on the assumptions listed above, the problem to be addressed in this paper is formulated as follows:

*Control Objective:* Given a quadrotor group with  $N$  agent with undirected graph  $\mathcal{G}$  and a set of reference trajectories generated by the virtual leader node with  $\eta_d = [x_d, y_d, z_d]^\top$  being the reference position,  $\psi_d$  being the reference yaw angle, and  $\nu_i = [\nu_{x,i}, \nu_{y,i}, \nu_{z,i}]^\top$  being the offset of the  $i$ -th quadrotor to  $\eta_d$ , design a type of adaptive controller such that for  $i = 1, 2, \dots, N$

$$\begin{aligned} \lim_{t \rightarrow T_\eta} \eta_i(t) - (\eta_d + \nu_i) &= 0, \\ \lim_{t \rightarrow T_\rho} \psi_i(t) - \psi_d &= 0, \end{aligned} \quad (12)$$

with  $T_\eta$  and  $T_\rho$  being the settling time of the translational and rotational subsystem, respectively.

## III. CONTROLLER DESIGN

### A. Rotational subsystem stability

For simplicity, the subscript “ $i$ ” in the rotational loop controller design is omitted since the quadrotors are all homogeneous and the design of the FTDO and FNTSMC in rotational loop does not require the information from other quadrotors. [33].

To begin with, a FTDO can be designed as

$$\begin{aligned} \dot{z}_{\rho 1} &= \nu_\rho m_{\rho 1} [\tilde{e}_\rho]^{\alpha_1} + (1 - \nu_\rho) n_{\rho 1} [\tilde{e}_\rho]^{\beta_1} \\ &\quad + z_{\rho 2}, \\ \dot{z}_{\rho 2} &= \nu_\rho m_{\rho 2} [\tilde{e}_\rho]^{\alpha_2} + (1 - \nu_\rho) n_{\rho 2} [\tilde{e}_\rho]^{\beta_2} \\ &\quad + z_{\rho 3} + A_\rho + B_\rho \tau, \\ \dot{z}_{\rho 3} &= \nu_\rho m_{\rho 3} [\tilde{e}_\rho]^{\alpha_3} + (1 - \nu_\rho) n_{\rho 3} [\tilde{e}_\rho]^{\beta_3}, \end{aligned} \quad (13)$$

where  $z_{\rho 1}$ ,  $z_{\rho 2}$ , and  $z_{\rho 3}$  are the estimations of  $e_\rho$ ,  $\dot{e}_\rho$ , and  $\Delta_\rho$ , respectively,  $\tilde{e}_{\rho,i} = e_\rho - z_{\rho i}$  is the estimation error of  $e_\rho$ .  $\nu_\rho$  is a switching parameter;  $\alpha_1$ ,  $\alpha_2$ ,  $\alpha_3$ ,  $\beta_1$ ,  $\beta_2$ , and  $\beta_3$  are positive constants. Specifically,  $\alpha_1 = \frac{3}{4}$ ,  $\alpha_2 = \frac{2}{4}$ ,  $\alpha_3 = \frac{1}{4}$ ,  $\beta_1 = \frac{5}{4}$ ,  $\beta_2 = \frac{6}{4}$ ,  $\beta_3 = \frac{7}{4}$ , and

$$\nu_\rho = \begin{cases} 0 & \|\tilde{e}_\rho\| > e_\rho^* \\ 1 & \|\tilde{e}_\rho\| < e_\rho^* \end{cases}$$

with  $e_\rho^*$  being the threshold of the estimation error. Apart from that, parameters  $m_{\rho 1}$ ,  $m_{\rho 2}$ ,  $m_{\rho 3}$ ,  $n_{\rho 1}$ ,  $n_{\rho 2}$ , and  $n_{\rho 3}$  are designed such that matrices

$$\Gamma_{m,\rho} = \begin{bmatrix} m_{\rho 1} & 1 & 0 \\ m_{\rho 2} & 0 & 1 \\ m_{\rho 3} & 0 & 0 \end{bmatrix} \text{ and } \Gamma_{n,\rho} = \begin{bmatrix} n_{\rho 1} & 1 & 0 \\ n_{\rho 2} & 0 & 1 \\ n_{\rho 3} & 0 & 0 \end{bmatrix}$$

are Hurwitz.

Given observer (13), the equivalent disturbance of the quadrotors, say,  $\Delta_\rho$ , can be estimate in fixed-time, which is denoted as  $\tilde{\Delta}_{\rho,i}$ , and the estimation error converges to a neighborhood of the origin  $\Omega_\rho$  [34] and [35].

Thereafter, a fast non-singular terminal sliding mode surface can be defined as

$$s_\rho = e_\rho + k_{\rho 1} e_\rho^{\frac{p_1}{p_2}} + k_{\rho 2} \dot{e}_\rho^{\frac{p_3}{p_4}}, \quad (14)$$

where  $k_{\rho 1} > 0$ ,  $k_{\rho 2} > 0$ .  $p_1$ ,  $p_2$ ,  $p_3$ , and  $p_4$  are all positive odd numbers satisfying

$$\frac{p_1}{p_2} > \frac{p_3}{p_4} > 1 \text{ and } 2 > \frac{p_3}{p_4} > 1.$$

Assuming there are no disturbances or uncertain terms in the system, an equivalent control law can be given by

$$\begin{aligned} \tau_{eq} &= -B_\rho^{-1} \left[ \tau_{eq,1} + \frac{p_4}{k_{\rho 2} p_3} \dot{e}_\rho^{2 - \frac{p_3}{p_4}} \circ \tau_{eq,2} \right], \\ \tau_{eq,1} &= A_\rho, \\ \tau_{eq,2} &= I_3 - \frac{k_{\rho 1} p_1}{p_3} e_\rho^{\frac{p_1}{p_2} - 1}. \end{aligned} \quad (15)$$

In addition, a switching control law is further required to maintain  $s_\rho$  at the origin when there exists disturbances or uncertainty in the system, which is given by

$$\tau_{sw} = -B_\rho^{-1} \left[ z_{\rho 3} + k_{\rho 3} \operatorname{sgn} s_\rho + k_{\rho 4} s_\rho^{\frac{p_5}{p_6}} \right], \quad (16)$$

where  $k_{\rho 3} > 0$ ,  $k_{\rho 4} > 0$  are positive constants.  $p_5 > p_6 > 1$  are all positive odd parameters. Then, the complete control law for the rotational loop can be designed as

$$\tau = \tau_{eq} + \tau_{sw}. \quad (17)$$

Based on the analysis and derivation aforementioned, the following theorem can be concluded.

*Theorem 1.* For the rotational subsystem of the quadrotor (3) disturbed by  $\Delta_\rho$ , the system is fixed-time stable with the FNTSMC designed in (17) and the FTDO introduced in (13).

*Proof.* Firstly, we need to prove that the sliding mode surface converges to the origin in finite-time.

Define Lyapunov function as  $V_{\rho 1} = \frac{1}{2} s_\rho^\top s_\rho$ . Differentiating  $V_{\rho 1}$  yields

$$\dot{V}_{\rho 1} = s_\rho^\top \left\{ \dot{e}_\rho + \frac{k_{\rho 1} p_1}{p_2} e_\rho^{\frac{p_1}{p_2}-1} \circ \dot{e}_\rho + \frac{k_{\rho 2} p_3}{p_4} e_\rho^{\frac{p_3}{p_4}-1} \circ [A_\rho + B_\rho (\tau_{eq} + \tau_{sw}) + \Delta_\rho] \right\} \quad (18)$$

Substituting controller (17) into  $\dot{V}_{\rho 1}$  and doing some manipulations yield

$$\dot{V}_{\rho 1} = s_\rho^\top \left[ \frac{k_{\rho 2} p_3}{p_4} e_\rho^{\frac{p_3}{p_4}-1} \circ \left( \Delta_\rho - z_{\rho 3} - k_{\rho 3} \operatorname{sgn} s_\rho - k_{\rho 4} s_\rho^{\frac{\alpha_{\rho 5}}{\alpha_{\rho 6}}} \right) \right]. \quad (19)$$

Denote  $\tilde{\Delta}_\rho = \Delta_\rho - z_{\rho 3}$  as the estimation error of  $\Delta_\rho$  and  $k_{\rho 0} = \frac{k_{\rho 2} p_3}{p_4} e_\rho^{\frac{p_3}{p_4}-1}$ , which yields

$$\begin{aligned} \dot{V}_{\rho 1} &= -k_{\rho 0}^\top \circ s_\rho^\top \left( k_{\rho 3} \operatorname{sgn} s_\rho + k_{\rho 4} s_\rho^{\frac{p_5}{p_6}} - \tilde{\Delta}_\rho \right) \\ &= -k_{\rho 4} k_{\rho 0}^\top s_\rho^{\frac{p_5+p_6}{p_6}} - k_{\rho, eq} k_{\rho 0}^\top |s_\rho| \end{aligned} \quad (20)$$

where  $k_{\rho, eq} = k_{\rho 3} - \|\tilde{\Delta}_\rho\|_2 > 0$ .

Note the fact that all elements in  $k_{\rho 0}$  are non-negative. Demoting the minimum element in  $k_{\rho 0}$  as  $\underline{k}_\rho$  and using Lemma 3 yield

$$\begin{aligned} \dot{V}_{\rho 1} &\leq -k_{\rho 4} \underline{k}_\rho \|s_\rho\|_2^{\frac{p_5+p_6}{2p_6}} - k_{\rho, eq} \underline{k}_\rho \|s_\rho\|_2^{\frac{1}{2}} \\ &= -k_{\rho 4} \underline{k}_\rho 2^{\frac{p_5+p_6}{2p_6}} V_{\rho 1}^{\frac{p_5+p_6}{2p_6}} - k_{\rho, eq} \underline{k}_\rho \sqrt{2} V_{\rho 1}^{\frac{1}{2}}. \end{aligned} \quad (21)$$

Using Lemma 2 and the fact  $p_5 > p_6$  yield that  $s_\rho$  is fixed-time stable, and the settling time is bounded by

$$T_{\rho 2} = \frac{\sqrt{2}}{k_{\rho, eq} \underline{k}_\rho} + \frac{p_6}{k_{\rho 4} \underline{k}_\rho (p_5 - p_6)} 2^{\frac{2p_6}{p_5-p_6}}. \quad (22)$$

Secondly, we need to prove that  $e_\rho$  converges to the origin in fixed-time when the states are maintained on the sliding mode surface. On the sliding mode surface, there is

$$e_\rho + k_{\rho 1} e_\rho^{\frac{p_1}{p_2}} + k_{\rho 2} \dot{e}_\rho^{\frac{p_3}{p_4}} = 0, \quad (23)$$

which yields

$$\dot{e}_\rho^{\frac{p_3}{p_4}} = -\frac{1}{k_{\rho 2}} \left( e_\rho + k_{\rho 1} e_\rho^{\frac{p_1}{p_2}} \right). \quad (24)$$

Define Lyapunov function as  $V_{\rho 2} = \frac{1}{2} e_\rho^\top e_\rho$ . Differentiating  $V_{\rho 2}$  along the system trajectory and using Lemma 3 yield

$$\begin{aligned} \dot{V}_{\rho 2} &= - \left[ \frac{1}{k_{\rho 2}} \left( e_\rho^\top \right)^{\frac{p_3}{p_4}} \left( e_\rho + k_{\rho 1} e_\rho^{\frac{p_1}{p_2}} \right) \right]^{\frac{p_4}{p_3}} \\ &\leq - \left[ \frac{1}{k_{\rho 2}} \|e_\rho\|_2^{\frac{p_3+p_4}{p_4}} + \frac{k_{\rho 1}}{k_{\rho 2}} \|e_\rho\|_2^{\frac{p_1+p_3}{p_2+p_4}} \right]^{\frac{p_4}{p_3}} \\ &= - \left[ \kappa_{\rho 1} V_{\rho 2}^{\frac{p_3+p_4}{2p_4}} + \kappa_{\rho 2} V_{\rho 2}^{\frac{1}{2} \left( \frac{p_1+p_3}{p_2+p_4} \right)} \right]^{\frac{p_4}{p_3}}, \end{aligned} \quad (25)$$

where  $\kappa_{\rho 1} = \frac{\sqrt{2(p_3+p_4)/p_4}}{k_{\rho 2}}$  and  $\kappa_{\rho 2} = \frac{k_{\rho 1} \sqrt{2p_1/p_2 + p_3/p_4}}{k_{\rho 2}}$ .

By using Lemma 2, one concludes  $e_\rho$  converges to the origin in a fixed-time, and the settling time can be bounded by

$$T_{\rho 3} = \frac{2p_3}{(p_3 - p_4)\kappa_{\rho 1}^{p_4/p_3}} + \frac{2p_2 p_3}{(p_1 p_4 - p_2 p_3) \kappa_{\rho 2}^{p_4/p_3}}. \quad (26)$$

Therefore, the convergence time of the system with external disturbance convergences within

$$T_\rho = T_{\rho 1} + T_{\rho 2} + T_{\rho 3}. \quad (27)$$

The proof is completed.  $\square$

*Remark 2.* In Eq. (14), there are

$$\frac{p_3 + p_4}{2p_4} \cdot \frac{p_4}{p_3} = \frac{p_3 + p_4}{2p_3} \in (0, 1),$$

and

$$\frac{1}{2} \left( \frac{p_1}{p_2} + \frac{p_3}{p_4} \right) \cdot \frac{p_4}{p_3} = \frac{1}{2} \left( \frac{p_1 p_4}{p_2 p_3} + 1 \right) > 1$$

hold, satisfying the conditions required in Lemma 2.

## B. Translational Subsystem Stability

Similarly, the fixed-time disturbance observer can be designed as

$$\begin{aligned} \dot{z}_{\eta 1, i} &= \nu_{\eta, i} m_{\eta 1, i} [\tilde{e}_{\eta 1, i}]^{\alpha_1} + (1 - \nu_{\eta, i}) n_{\eta 1, i} [\tilde{e}_{\eta 1, i}]^{\beta_1} \\ &\quad + z_{\eta 2, i}, \\ \dot{z}_{\eta 2, i} &= \nu_{\eta, i} m_{\eta 2, i} [\tilde{e}_{\eta 1, i}]^{\alpha_2} + (1 - \nu_{\eta, i}) n_{\eta 2, i} [\tilde{e}_{\eta 1, i}]^{\beta_2} \\ &\quad + z_{\eta 3, i} - \frac{k_t}{m_i} \dot{\eta}_i + u_{\eta, i}, \\ \dot{z}_{\eta 3, i} &= \nu_{\eta, i} m_{\eta 3, i} [\tilde{e}_{\eta 1, i}]^{\alpha_3} + (1 - \nu_{\eta, i}) n_{\eta 3, i} [\tilde{e}_{\eta 1, i}]^{\beta_3}, \end{aligned} \quad (28)$$

where  $z_{\eta 1, i}$ ,  $z_{\eta 2, i}$ , and  $z_{\eta 3, i}$  are the estimation of  $e_{\eta, i}$ ,  $\dot{e}_{\eta, i}$ , and  $\Delta_{\eta, i}$ , respectively,  $\tilde{e}_{\eta 1, i} = e_{\eta, i} - z_{\eta 1, i}$  is the estimation error of  $e_{\eta, i}$ . Specifically,  $\alpha_1 = \frac{3}{4}$ ,  $\alpha_2 = \frac{2}{4}$ ,  $\alpha_3 = \frac{1}{4}$ ,  $\beta_1 = \frac{5}{4}$ ,  $\beta_2 = \frac{6}{4}$ ,  $\beta_3 = \frac{7}{4}$ , and

$$\nu_{\eta, i} = \begin{cases} 0 & \|\tilde{e}_{\eta, i, 1}\| > e_{\eta, i}^*, \\ 1 & \|\tilde{e}_{\eta, i, 1}\| < e_{\eta, i}^* \end{cases}$$

with  $e_{\eta, i}^*$  being the threshold of the estimation error. Apart from that, hyper-parameters  $m_{\eta 1, i}$ ,  $m_{\eta 2, i}$ ,  $m_{\eta 3, i}$ ,  $n_{\eta 1, i}$ ,  $n_{\eta 2, i}$ , and  $n_{\eta 3, i}$  are designed such that matrices

$$\Gamma_{m, \eta, i} = \begin{bmatrix} m_{\eta 1, i} & 1 & 0 \\ m_{\eta 2, i} & 0 & 1 \\ m_{\eta 3, i} & 0 & 0 \end{bmatrix}, \quad \Gamma_{n, \eta, i} = \begin{bmatrix} n_{\eta 1, i} & 1 & 0 \\ n_{\eta 2, i} & 0 & 1 \\ n_{\eta 3, i} & 0 & 0 \end{bmatrix}$$

are Hurwitz. Similarly,  $\Delta_{\eta,i}$  can be estimated in fixed-time  $T_{\eta1,i}$ , and the estimation error converges to a neighborhood of the origin  $\Omega_{\eta,i}$  [34], [35].

Thereafter, a fast non-singular terminal sliding mode surface for the  $i$ -th quadrotor can be defined as

$$s_{\eta,i} = e_{\eta,i} + k_{\eta1,i} e_{\eta,i}^{\frac{q_1}{q_2}} + k_{\eta2,i} \dot{e}_{\eta,i}^{\frac{q_3}{q_4}}, \quad (29)$$

where  $k_{\eta1,i} > 0$ ,  $k_{\eta2,i} > 0$ .  $q_1$ ,  $q_2$ ,  $q_3$ , and  $q_4$  are all positive odd numbers satisfying

$$\frac{q_1}{q_2} > \frac{q_3}{q_4} > 1 \text{ and } 2 > \frac{q_3}{q_4} > 1.$$

An equivalent control law is then proposed to maintain  $s_{\eta,i}$  on the sliding mode surface, which is given by

$$\begin{aligned} u_{\eta,i,eq} &= -\frac{1}{b_i + d_i} (u_{\eta,i,eq1} + u_{\eta,i,eq2}), \\ u_{\eta,i,eq1} &= -\frac{(b_i + d_i) k_{t,i} \dot{\eta}_i - \Lambda_{i0}}{m_i}, \\ u_{\eta,i,eq2} &= \frac{q_4}{q_3 k_{\eta2,i}} \dot{\eta}_i^{2-\frac{q_3}{q_4}} \circ \left( I_3 - \frac{q_1 k_{\eta1,i}}{q_2} e_{\eta,i}^{\frac{q_1}{q_2}-1} \right). \end{aligned} \quad (30)$$

Further, considering the uncertain parts and external disturbances acted on the translational subsystem, a switching control law is required, which is designed as

$$\begin{aligned} u_{\eta,i,sw} &= -\frac{1}{b_i + d_i} (u_{\eta,i,sw1} + u_{\eta,i,sw2}), \\ u_{\eta,i,sw1} &= (b_i + d_i) z_{\eta3,i} + \sum_{i=1}^N a_{ij} z_{\eta3,j}, \\ u_{\eta,i,sw2} &= k_{\eta3,i} \operatorname{sgn} s_{\eta,i} - k_{\eta4,i} s_{\eta,i}^{\frac{q_5}{q_6}}. \end{aligned} \quad (31)$$

Finally, the complete control law is given by

$$u_{\eta,i} = u_{\eta,i,eq} + u_{\eta,i,sw}. \quad (32)$$

Similar to that of rotational subsystem, a theorem is then illustrated to guarantee the stability of the translational subsystem of the entire quadrotor group.

**Theorem 2.** For the consensus tracking error of the translational subsystems of the quadrotor formation (11) disturbed by  $\Delta_i$ , the system is fixed-time stable with FNTSMC (32) and FTDO (28).

*Proof.* Firstly, we need to prove  $s_{\eta,i}$ ,  $i = 1, 2, \dots, N$  converge to the origin in fixed-time. Define Lyapunov function as  $V_{\eta1} = \frac{1}{2} \sum_{i=1}^N s_{\eta,i}^\top s_{\eta,i}$ . Differentiating  $V_{\eta1}$  yields

$$\begin{aligned} \dot{V}_{\eta1} &= \sum_{i=1}^N s_{\eta,i}^\top \dot{s}_{\eta,i} \\ &= \sum_{i=1}^N s_{\eta,i}^\top \left( \dot{e}_{\eta,i} + \frac{q_1 k_{\eta1,i}}{q_2} e_{\eta,i}^{\frac{q_1}{q_2}-1} \circ \dot{e}_{\eta,i} + \right. \\ &\quad \left. + \frac{q_3 k_{\eta3,i}}{q_4} \dot{e}_{\eta,i}^{\frac{q_3}{q_4}-1} \circ \ddot{e}_{\eta,i} \right). \end{aligned} \quad (33)$$

Substituting Eq. (11) into  $\dot{V}_{\eta1}$ , using controller (32), and doing some manipulations yield

$$\begin{aligned} \dot{V}_{\eta1} &= \sum_{i=1}^N s_{\eta,i}^\top \left\{ \dot{e}_{\eta,i} + \frac{q_1 k_{\eta1,i}}{q_2} e_{\eta,i}^{\frac{q_1}{q_2}-1} \circ \dot{e}_{\eta,i} + \right. \\ &\quad + \frac{q_3 k_{\eta3,i}}{q_4} \dot{e}_{\eta,i}^{\frac{q_3}{q_4}-1} \left[ -\frac{(b_i + d_i) k_{t,i}}{m_i} \dot{\eta}_i + (b_i + d_i) u_{\eta,i} \right. \\ &\quad \left. - \Lambda_{i0} + (b_i + d_i) \Delta_{\eta,i} - \sum_{j=i}^N a_{ij} \Delta_{\eta,j} \right] \left. \right\} \\ &= \sum_{i=1}^N s_{\eta,i}^\top \left\{ \frac{q_3 k_{\eta2,i}}{q_4} \dot{e}_{\eta,i}^{\frac{q_3}{q_4}-1} \circ \left[ (b_i + d_i) (\Delta_{\eta,i} - z_{\eta3,i}) \right. \right. \\ &\quad \left. \left. + \sum_{j=i}^N a_{ij} (z_{\eta3,j} - \Delta_{\eta,j}) \right] \right\}. \end{aligned} \quad (34)$$

Define the estimation error of  $\Delta_{\eta,i}$  as  $\tilde{\Delta}_{\eta,i} = \Delta_{\eta,i} - z_{\eta3,i}$  and  $k_{\eta0,i} = \frac{q_3 k_{\eta2,i}}{q_4} \dot{e}_{\eta,i}^{\frac{q_3}{q_4}-1}$ .  $\dot{V}_{\eta1}$  can be simplified as

$$\begin{aligned} \dot{V}_{\eta1} &= -\sum_{i=1}^N k_{\eta0,i}^\top \circ s_{\eta,i}^\top \left\{ \left[ k_{\eta3,i} \operatorname{sgn} s_{\eta,i} + k_{\eta4,i} s_{\eta,i}^{\frac{q_5}{q_6}} \right. \right. \\ &\quad \left. \left. - (b_i + d_i) \tilde{\Delta}_{\eta,i} - \sum_{j=i}^N a_{ij} \tilde{\Delta}_{\eta,j} \right] \right\}. \end{aligned} \quad (35)$$

Note the fact the all elements in  $k_{\eta0,i}$  are non-negative. Using Lemma 3 and denoting the minimum element in  $k_{\eta0,i}$  as  $\underline{k}_{\eta,i}$  yield

$$\begin{aligned} \dot{V}_{\eta1} &\leq -\sum_{i=1}^N \underline{k}_{\eta,i} s_{\eta,i}^\top \left\{ \left[ k_{\eta3,i} \operatorname{sgn} s_{\eta,i} + k_{\eta4,i} s_{\eta,i}^{\frac{q_5}{q_6}} \right. \right. \\ &\quad \left. \left. - (b_i + d_i) \tilde{\Delta}_{\eta,i} - \sum_{j=i}^N a_{ij} \tilde{\Delta}_{\eta,j} \right] \right\} \\ &= -\sum_{i=1}^N \underline{k}_{\eta,i} s_{\eta,i}^\top \left\{ k_{\eta3,i} \operatorname{sgn} s_{\eta,i} + k_{\eta4,i} s_{\eta,i}^{\frac{q_5}{q_6}} \right\} \\ &= -\sum_{i=1}^N \underline{k}_{\eta,i} \left\{ k_{\eta3,i} \sum_{j=1}^3 |s_{\eta,i,j}| + k_{\eta4,i} \sum_{j=1}^3 |s_{\eta,i,j}|^{1+\frac{q_5}{q_6}} \right\} \\ &\leq -\sum_{i=1}^N \underline{k}_{\eta,i} \left\{ k_{\eta3,i} \|s_{\eta,i}\|_2^{\frac{1}{2}} + k_{\eta4,i} \|s_{\eta,i}\|_2^{\frac{1}{2}(1+\frac{q_5}{q_6})} \right\} \\ &\leq -k_{\eta3} \sum_{i=1}^N \sum_{j=1}^3 |s_{\eta,i,j}| - k_{\eta4} \sum_{i=1}^N \sum_{j=1}^3 |s_{\eta,i,j}|^{1+\frac{q_5}{q_6}}, \end{aligned} \quad (36)$$

where  $\underline{k}_{\eta3} = \min(k_{\eta,i}, k_{\eta3,i})$ ,  $\underline{k}_{\eta4} = \min(k_{\eta,i}, k_{\eta4,i})$ , and  $k_{\eta,i} = k_{\eta3,i} - (b_i + d_i) \|\tilde{\Delta}_{\eta,i}\|_2 - \sum_{j=1}^N a_{ij} \|\tilde{\Delta}_{\eta,j}\|_2 > 0$  for

$i = 1, 2, \dots, N$ . Using Lemma 3 again in Eq. (36) yields

$$\begin{aligned}\dot{V}_{\eta 1} &\leq -k_{\eta 3} \sum_{i=1}^N \left( \|s_{\eta, i}\|_2^2 \right)^{\frac{1}{2}} - k_{\eta 4} \sum_{i=1}^N \left( \|s_{\eta, i}\|_2^2 \right)^{\frac{1}{2}(1+\frac{q_5}{q_6})} \\ &= -k_{\eta 3} \left( \sum_{i=1}^N \|s_{\eta, i}\|_2^2 \right)^{\frac{1}{2}} - k_{\eta 4} \left( \sum_{i=1}^N \|s_{\eta, i}\|_2^2 \right)^{\frac{1}{2}(1+\frac{q_5}{q_6})} \\ &= -\kappa_{\eta 1} V_{\eta 1}^{\frac{1}{2}} - \kappa_{\eta 2} V_{\eta 1}^{\frac{1}{2}(1+\frac{q_5}{q_6})},\end{aligned}\quad (37)$$

where  $\kappa_{\eta 1} = k_{\eta 3} \sqrt{2}$  and  $\kappa_{\eta 2} = k_{\eta 4} \sqrt{2(q_6+q_5)/q_6}$ . Using Lemma 2 yields that  $s_{\eta, i}, i = 1, 2, \dots, N$  are fixed-time stable, and the settling time can be bounded by

$$T_{\eta 2} = \frac{2}{\kappa_{\eta 1}} + \frac{2q_6}{\kappa_{\eta 2}(q_5 - q_6)}. \quad (38)$$

Secondly, similar to that of the rotational subsystem, we need to prove that the tracking errors of the quadrotor group converge to the origin in fixed time. On the sliding mode surface, there is

$$s_{\eta, i} = e_{\eta, i} + k_{\eta 1, i} e_{\eta, i}^{\frac{q_1}{q_2}} + k_{\eta 2, i} \dot{e}_{\eta, i}^{\frac{q_3}{q_4}} = 0, \quad (39)$$

which yields

$$\dot{e}_{\eta, i}^{\frac{q_3}{q_4}} = -\frac{1}{k_{\eta 2, i}} \left( e_{\eta, i} + k_{\eta 1, i} e_{\eta, i}^{\frac{q_1}{q_2}} \right). \quad (40)$$

The Lyapunov function can be defined as  $V_{\eta 2} = \frac{1}{2} \sum_{i=1}^N e_{\eta, i}^\top e_{\eta, i}$ . Differentiating  $V_{\eta 2}$  yields

$$\begin{aligned}\dot{V}_{\eta 2} &= - \sum_{i=1}^N \left[ \frac{1}{k_{\eta 2, i}} (e_{\eta, i}^\top)^{\frac{q_3}{q_4}} \left( e_{\eta, i} + k_{\eta 1, i} e_{\eta, i}^{\frac{p_1}{p_2}} \right) \right]^{\frac{q_4}{q_3}} \\ &= - \sum_{i=1}^N \left[ \frac{1}{k_{\eta 2, i}} \left( \|e_{\eta, i}\|_2^2 \right)^{\frac{1}{2}(1+\frac{q_3}{q_4})} \right. \\ &\quad \left. + \frac{k_{\eta 1, i}}{k_{\eta 2, i}} \left( \|e_{\eta, i}\|_2^2 \right)^{\frac{1}{2}(\frac{q_3}{q_4} + \frac{q_1}{q_2})} \right]^{\frac{q_4}{q_3}}.\end{aligned}\quad (41)$$

Using Lemma 3 yields

$$\begin{aligned}\dot{V}_{\eta 2} &\leq - \left\{ \sum_{i=1}^N \left[ \frac{1}{k_{\eta 2, i}} \left( \|e_{\eta, i}\|_2^2 \right)^{\frac{1}{2}(1+\frac{q_3}{q_4})} \right. \right. \\ &\quad \left. \left. + \frac{k_{\eta 1, i}}{k_{\eta 2, i}} \left( \|e_{\eta, i}\|_2^2 \right)^{\frac{1}{2}(\frac{q_3}{q_4} + \frac{q_1}{q_2})} \right] \right\}^{\frac{q_4}{q_3}} \\ &\leq - \left[ \frac{1}{\bar{k}_{\eta 2}} \left( \sum_{i=1}^N \|e_{\eta, i}\|_2^2 \right)^{\frac{1}{2}(1+\frac{q_3}{q_4})} \right. \\ &\quad \left. + \frac{k_{\eta 1}}{\bar{k}_{\eta 2}} \left( \sum_{i=1}^N \|e_{\eta, i}\|_2^2 \right)^{\frac{1}{2}(\frac{q_3}{q_4} + \frac{q_1}{q_2})} \right]^{\frac{q_4}{q_3}} \\ &= - \left[ \kappa_{\eta 1} V_{\eta 2}^{\frac{1}{2}(1+\frac{q_3}{q_4})} + \kappa_{\eta 2} V_{\eta 2}^{\frac{1}{2}(\frac{q_3}{q_4} + \frac{q_1}{q_2})} \right]^{\frac{q_4}{q_3}},\end{aligned}\quad (42)$$

where  $\bar{k}_{\eta 2} = \max(k_{\eta 1, i}, k_{\eta 2, i}, \dots, k_{\eta N, i})$ ,  $\kappa_{\eta 1} = 2^{(\frac{1}{2} + \frac{q_3}{2q_4})/\bar{k}_{\eta 2}}$ ,  $\kappa_{\eta 2} = \min(k_{\eta 1, i}, k_{\eta 2, i}, \dots, k_{\eta N, i})$ , and

### Algorithm 1 PPO with GAE

---

```

Input Episode index  $ep = 0$ , maximum learning episode  $N_e$ , initial critic net  $cr()$ , initial actor net  $ac()$ .
1: while  $ep < N_e$  do
2:   Data Collection, compute the log-probability of the actor  $ac_l$ 
3:    $V = cr(s), V' = cr(s')$ 
4:   Compute the GAE:  $gae()$ 
5:   Compute the advantage function:  $adv()$ 
6:    $V_{target} = adv() + V$ 
7:   Get the distribution of actor:  $\mathcal{N}_{ac}$ 
8:   Get entropy:  $en = \mathcal{N}_{ac}.get\_entropy()$ 
9:   Get log-probability:  $log\_prob = \mathcal{N}_{ac}.log\_prob()$ 
10:   $ra = e^{log\_prob - ac_l}$ 
11:   $s_1 = ra * adv, s_2 = adv * [ra.clip(c_{min}, c_{max})]$ 
12:  Compute loss function:  $l_{ac} = -\min(s_1, s_2) - en * en$ 
13:  Update actor net:  $ac().update()$ 
14:  Compute loss function:  $l_{cr} = mse\_loss(V_{target}, V)$ 
15:  Update critic net:  $cr().update()$ 
16:   $ep += 1$ 
17: return  $cr(), ac()$ 
```

---

$\kappa_{\eta 2} = k_{\eta 2} 2^{(\frac{q_3}{2q_4} + \frac{q_1}{2q_2})/\bar{k}_{\eta 2}}$ . Using Lemma 2 indicates the  $e_{\eta, i}, i = 1, 2, \dots, N$  converge to the origin in a fixed-time  $T_{\eta 3}$ , which can be bounded by

$$T_{\eta 3} = \frac{2q_3}{(q_3 - q_4)\kappa_{\eta 2}^{q_4/q_3}} + \frac{2q_2q_3}{(q_1q_4 - q_2q_3)\kappa_{\eta 2}^{q_4/q_3}}. \quad (43)$$

Therefore, the translational subsystem of the quadrotor group is fixed-time stable, and the settling time can be bounded by

$$T_\eta = T_{\eta 1} + T_{\eta 2} + T_{\eta 3}. \quad (44)$$

The proof is completed.  $\square$

### IV. DRL FOR PARAMETER OPTIMIZATION

In Section III, a consensus control protocol is designed for both the rotational and translational subsystems of the quadrotors. However, tuning the hyperparameters remains a critical issue that needs to be addressed. In this section, deep reinforcement learning (DRL) is utilized as a hyperparameter optimizer for fast nonsingular terminal sliding mode controllers (FNTSMCs) to achieve improved control performance.

The basic deep reinforcement learning (DRL) algorithm employed in this study is Proximal Policy Optimization (PPO) [36], which is an engineering approximation of Trust Region Policy Optimization (TRPO). TRPO aims to achieve monotonic improvement of the policy during the iterative learning process by integrating Policy Gradient (PG) [37], Natural Policy Gradient (NPG) [38], and Conservative Policy Iteration (CPO) [39] into a unified learning framework. However, implementing pure TRPO is challenging due to the complexity of calculating the Hessian matrix in real time. Therefore, PPO is a more popular choice for real-world applications. Specifically, an improved version of PPO, referred to as PPO with Generalized Advantage Estimation (GAE) [40], is

TABLE I  
SOME RELATED PARAMETERS OF THE PPO OPTIMIZER.

Symbol	Value	Symbol	Value
$T_m$	10	$dt$	0.01
$std_0$	0.45	$std_{min}$	0.2
$std_d$	0.05	$std_{dN}$	250
$\gamma$	0.99	$K_{ep}$	10
$b_s$	$T_m/dt * 2$	$al_r$	$10^{-4}$
$c_{lr}$	$10^{-3}$	$en_c$	0.01
$\lambda$	0.95	$c_{min}, c_{max}$	0.8, 1.2

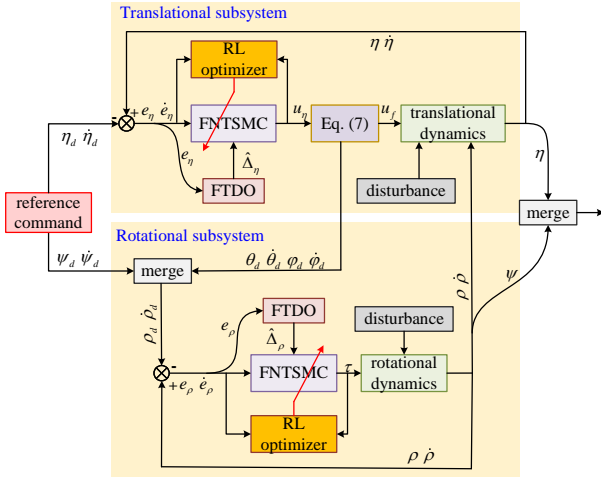


Fig. 1. Diagram of the learning-based control framework

selected as the learning framework. Table I lists some related parameters of PPO.

In Table I,  $T_m$  represents the maximum simulation time of an episode, and  $dt$  is the sampling period.  $std_0$ ,  $std_{min}$ ,  $std_d$ , and  $std_{dN}$  are parameters for tuning the standard deviation in the Gaussian exploration policy.  $N_m$  is the maximum number of learning episodes,  $\gamma$  is the discount factor,  $K_{ep}$  is the number of times the neural network (NN) gradient descends in one learning iteration, and  $b_s$  is the buffer size.  $al_r$  and  $c_{lr}$  denote the learning rates of the actor and critic networks, respectively.  $en_c$ ,  $\lambda$ ,  $c_{min}$ , and  $c_{max}$  are parameters used in the Generalized Advantage Estimation (GAE) technique, as referenced in [40]. Additionally,  $N_m = 1000 \cdot \frac{(std_0 - std_{min})}{std_d} + 1000$  is the maximum training episode. The pseudocode for PPO with GAE is illustrated in Algorithm 1. The fundamentals of the PPO algorithm can be found in [36] and various highly-stared GitHub repositories.

The diagram of the learning-based control framework for a single quadrotor is demonstrated in Fig. 1. In Fig. 1, the rotational and translational loop controls are coupled and connected with the desired roll and pitch angles, denoted as  $\phi_d$  and  $\theta_d$ . The hyperparameters of the FNTSMCs for both loops are optimized by deep reinforcement learning (DRL) simultaneously and separately.

#### A. Rotational Subsystem Parameter Optimizer Training

The controller for the rotational subsystem is utilized in Eq. (17) and is tuned by  $k_{\rho 1,i}$ ,  $k_{\rho 2,i}$ ,  $k_{\rho 3,i}$ ,  $k_{\rho 4,i}$ , and  $p_1 \sim p_6$ . First, to ensure the rapid convergence of the training process,

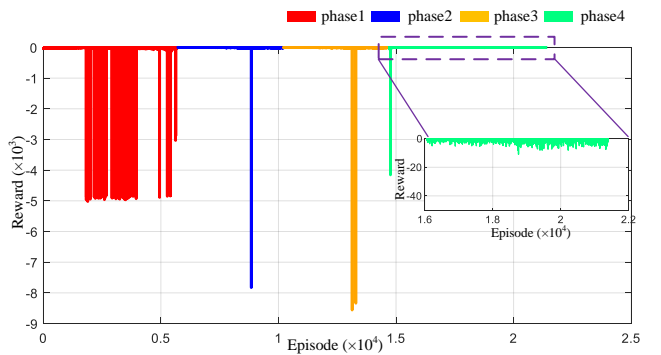


Fig. 2. Reward of the training process of rotational subsystem.

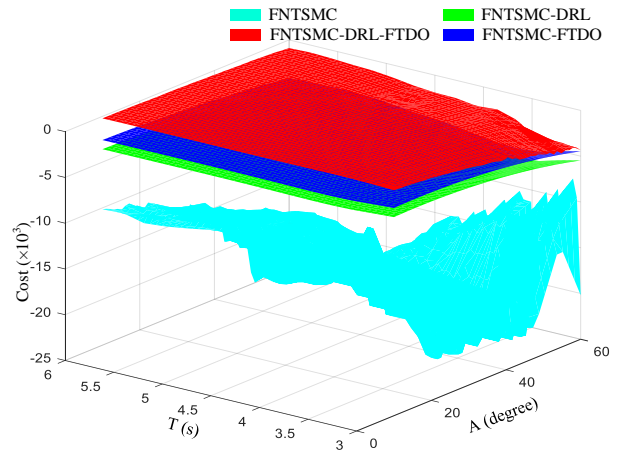


Fig. 3. Comparative cost surface under different control frameworks and different initial conditions.

we select  $p_1 = 9$ ,  $p_2 = 7$ ,  $p_3 = 5$ ,  $p_4 = 3$ ,  $p_5 = 7$ , and  $p_6 = 5$ . Second, to reduce the gap between numerical simulations and real-world experiments, we opted not to rely solely on the results learned by DRL. Specifically, the regulation of  $k_{\rho 1,i}$ ,  $k_{\rho 2,i}$ , and  $k_{\rho 4,i}$  is assigned to DRL, while  $k_{\rho 3,i}$  is retained to further enhance the robustness of the controller during real-world experiments.

Therefore, the input and output of the optimizer for rotational subsystem are respectively defined as

$$\begin{aligned}\chi_{\rho,i} &= [e_{\rho,i}^\top, \dot{e}_{\rho,i}^\top]^\top \in \mathbb{R}^6, \\ \Theta_{\rho,i} &= [k_{\rho 1,i,x}, k_{\rho 1,i,y}, k_{\rho 1,i,z}, k_{\rho 2,i,x}, \\ &\quad k_{\rho 2,i,y}, k_{\rho 2,i,z}, k_{\rho 3,i,x}, k_{\rho 3,i,y}, k_{\rho 3,i,z}]^\top \in \mathbb{R}^9.\end{aligned}\quad (45)$$

The reward function is defined as

$$J_{\rho,i}(t) = \int_{t=0}^{\infty} (\chi_{\rho,i}^\top Q_{\rho,i} \chi_{\rho,i} + \tau^\top R_{\rho,i} \tau) dt, \quad (46)$$

where  $Q_{\rho,i} = \text{diag}(Q_{e_{\rho,i}}, Q_{\dot{e}_{\rho,i}})$  with  $Q_{e_{\rho,i}} = \mathbf{I}_3$ ,  $Q_{\dot{e}_{\rho,i}} = 0.01\mathbf{I}_3$  and  $R_{\rho,i} = 0.01\mathbf{I}_3$ .

The curves for reward during the training process are shown in Fig. 2, where a multi-stage training technique [41] is employed to simultaneously accelerate the training process and improve the robustness of the trained neural network (NN). Specifically, during the first training stage, the control performance fluctuates significantly because the NNs have not fully

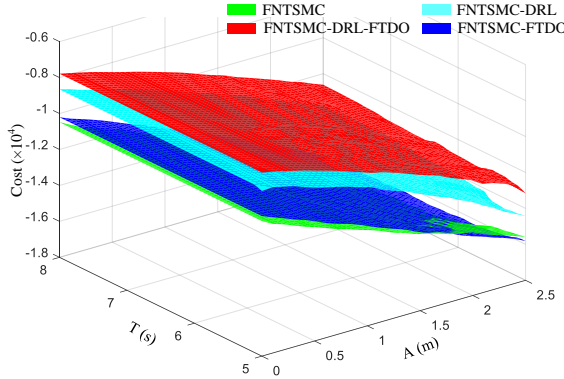


Fig. 4. Comparative cost surface under different control frameworks and different initial conditions.

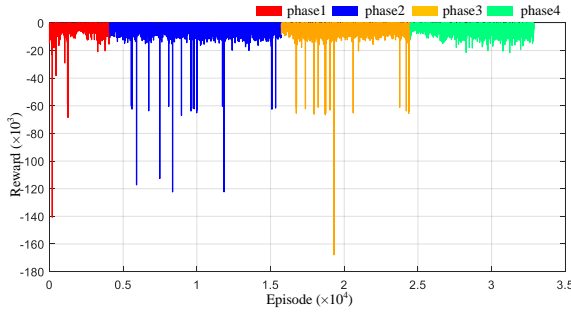


Fig. 5. Reward of the training process of translational subsystem.

converged. Therefore, in the subsequent three training stages, the initial policies are set to the results from the corresponding previous training stage. Additionally, lower learning rates for the NNs are chosen to reduce fluctuations and enhance the robustness of the learned optimizer.

Moreover, we further collected the costs associated with the rotational subsystem control under various initial conditions and different control frameworks to preliminarily demonstrate the superiority of our proposed control framework. This is shown in Fig. 3, which clearly indicates that the proposed FNTSMC-DRL-FTDO control framework outperforms the controllers that do not utilize the DRL technique. Notably, the performance of the pure FNTSMC (without FTDO or DRL) exhibits significant fluctuations due to the strong external disturbances applied to the system, which indirectly highlights the robustness of the proposed control framework.

*Remark 3.* In order to obtain a DRL-based optimizer more quickly, the neural networks are trained in a single-agent interactive environment, as all quadrotors are homogeneous. The well-trained NN-based optimizer is integrated into the FNTSMC of each quadrotor during numerous validations and physical experiments to tune the hyper-parameters of the FNTSMCs in real-time.

### B. Translational Subsystem Parameter Optimizer Training

Similarly, we set  $q_1 = 9$ ,  $q_2 = 7$ ,  $q_3 = 5$ ,  $q_4 = 3$ ,  $q_5 = 7$ , and  $q_6 = 5$ . and  $k_{\eta 3,i}$  is retained out of the DRL-based

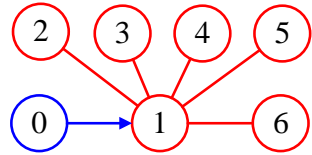


Fig. 6. Topological graph of simulation group 1.

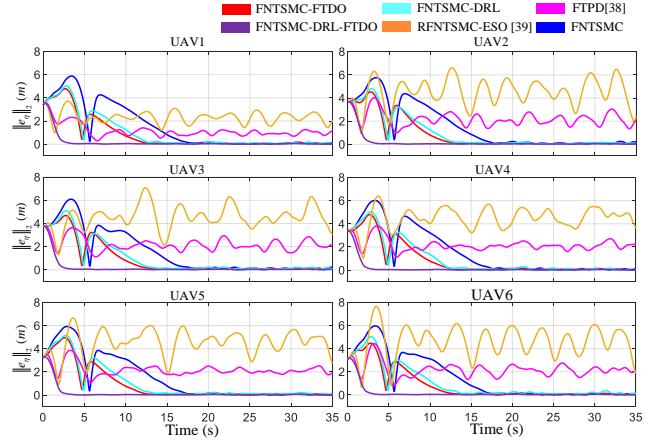


Fig. 7.  $\|e_{\eta,i}\|_2$  of each quadrotor under different control frameworks.

optimization framework. The input and output of the optimizer of translational subsystem are respectively defined as

$$\begin{aligned} \chi_{\eta,i} &= [e_{\eta,i}^\top, \dot{e}_{\eta,i}^\top]^\top \in \mathbb{R}^6, \\ \Theta_{\eta,i} &= \left[ k_{\eta 1,i,x}, k_{\eta 1,i,y}, k_{\eta 1,i,z}, k_{\eta 2,i,x}, \right. \\ &\quad \left. k_{\eta 2,i,y}, k_{\eta 2,i,z}, k_{\eta 3,i,x}, k_{\eta 3,i,y}, k_{\eta 3,i,z} \right]^\top \in \mathbb{R}^9. \end{aligned} \quad (47)$$

The reward function is defined as

$$J_{\eta,i}(t) = \int_{t=0}^{\infty} (\chi_{\eta,i}^\top Q_{\eta,i} \chi_{\eta,i} + u_{\eta,i}^\top R_{\eta,i} u_{\eta,i}) dt, \quad (48)$$

where  $Q_{\eta,i} = \text{diag}(Q_{e_{\eta,i}}, Q_{\dot{e}_{\eta,i}})$  with  $Q_{e_{\eta,i}} = \mathbf{I}_3$  and  $Q_{\dot{e}_{\eta,i}} = 0.1\mathbf{I}_3$  and  $R_{\eta,i} = 0.01\mathbf{I}_3$ .

The curves for the reward during the training process are recorded in Fig. 5. The trend of the reward curve is very similar to that of the rotational subsystem. The cost surfaces of the translational subsystem control under different initial conditions and various control frameworks are presented in Fig. 4, which reveals that the patterns of translational control performance are fundamentally similar to those of the rotational loop. The performance of the proposed FNTSMC-DRL-FTDO control framework outperforms the other three methods. Additionally, it is clear that the cost of the FNTSMC (represented by the green surface) is lower than that of FNTSMC-DRL (represented by the cyan surface), further indicating the superiority of the DRL technique.

## V. SIMULATION

### A. Simulation Group 1

The topological graph is shown in Fig. 6. Correspondingly, the adjacent matrix  $\mathcal{A}_{s1}$ , in-degree matrix  $\mathcal{D}_{s1}$ , communication matrix  $\mathcal{B}_{s1}$ , and Laplacian matrix  $\mathcal{L}_{s1}$  are respectively defined

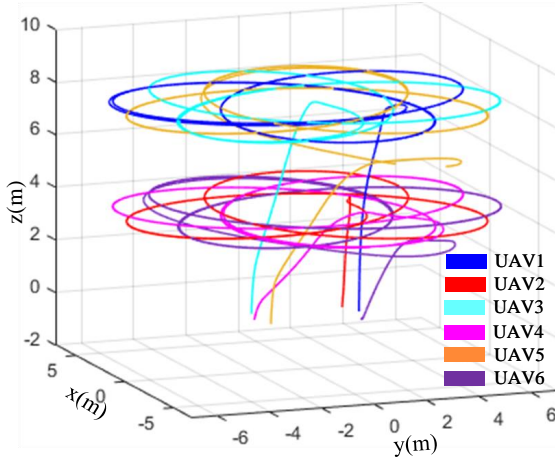


Fig. 8. Graphic demonstration of the quadrotor formation in a 3D view.

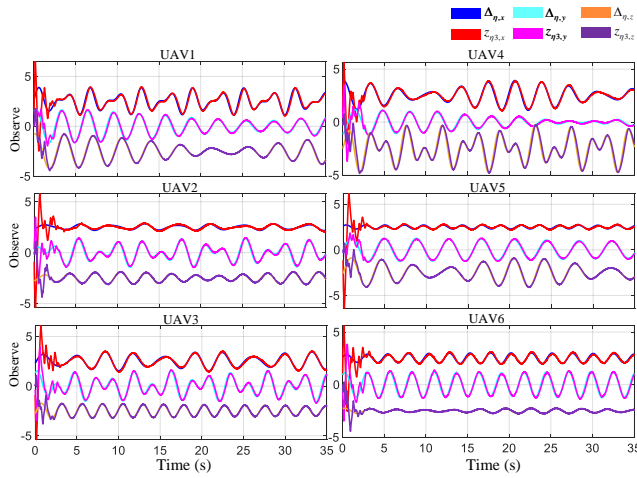


Fig. 9. Output of the observers.

as  $\mathcal{A}_{s1} = [0, 1, 1, 1, 1, 1; 1, 0, 0, 0, 0, 0; 1, 0, 0, 0, 0, 0; 1, 0, 0, 0, 0, 0; 0, 0, 1, 0, 0, 0; 1, 0, 0, 0, 0, 0]$ ,  $\mathcal{D}_{s1} = \text{diag}(5, 1, 1, 1, 1, 1)$ ,  $\mathcal{B}_{s1} = \text{diag}(1, 0, 0, 0, 0, 0)$ , and  $\mathcal{L}_{s1} = \mathcal{D}_{s1} - \mathcal{A}_{s1}$ .

The equation of the geometric center  $\mathcal{O}_d$  is defined as

$$\begin{aligned} x_d &= r_d \sin 0.2\pi t + 2, \\ y_d &= r_d \cos 0.2\pi t + 3, \\ z_d &= \sin 0.4\pi t + 2 \end{aligned} \quad (49)$$

with  $r_d = 5m$ . The offsets of each quadrotor to  $\mathcal{O}_d$ , denoted by  $\nu_i, i = 1, 2, \dots, 6$ , are defined as

$$\begin{aligned}\nu_{i,x} &= r_\nu \sin(0.2\pi t + \phi_{x,i}), \\ \nu_{i,y} &= r_\nu \sin(0.2\pi t + \phi_{y,i}), \\ \nu_{i,z} &= 0,\end{aligned}\tag{50}$$

where  $\phi_{x,i} = \frac{\pi}{2} + (i-1)\frac{\pi}{3}$ ,  $\phi_{y,i} = (i-1)\frac{\pi}{3}$  and  $r_\nu = 2m$ .

Fig. 7 illustrates the 2-norm of the tracking errors under six different control frameworks, clearly demonstrating that the purple curve exhibits the best performance. The red curve also converges to the origin eventually; however, due to the absence of a parameter adaptive adjustment mechanism, fluctuations are quite noticeable at the beginning. Other controllers can

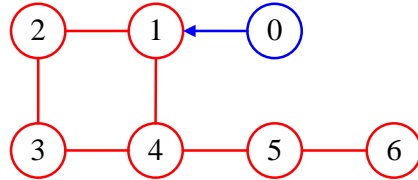


Fig. 10. Topological graph of simulation group 2.

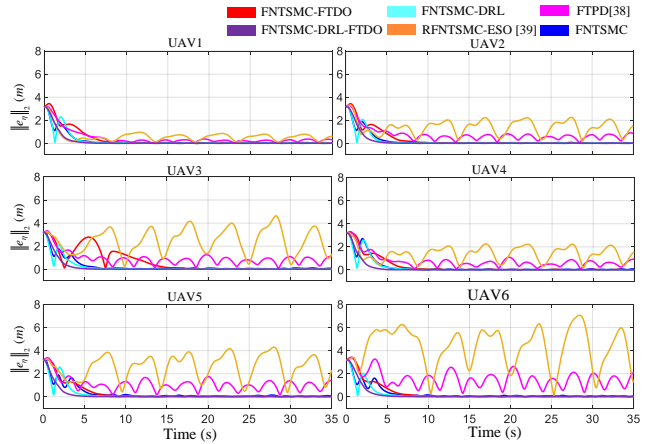


Fig. 11.  $\|e_\eta\|_2$  of each quadrotor under different control frameworks.

ensure system stability, but they consistently exhibit relatively large tracking errors.

We further conduct a simulation in which the reference trajectories along the XOY plane remain unchanged while the altitude is set to different constant values. The corresponding position response of the quadrotor group under the control framework “FNTSMC+RL+FTDO” is demonstrated in Fig. 8, where the reference trajectories are the superposition of two circles with different radii.

Correspondingly, the output of the FTDOs is illustrated in Fig. 9. Fig. 9 clearly demonstrates that the FTDO can accurately track the external disturbances in fixed time (about 1 second). The disturbances set in the simulation consist of combinations of sine functions with varying amplitudes, phases, and periods. Therefore, the FTDO can provide a precise estimation of the unknown items affecting the quadrotors.

### B. Simulation Group 2

We further test our algorithm with a more complicated topological graph and a more aggressive reference trajectory. The topological graph of simulation group 2 is shown in Fig. 10. Correspondingly, the adjacency matrix  $\mathcal{A}_{s2}$ , in-degree matrix  $\mathcal{D}_{s2}$ , communication matrix  $\mathcal{B}_{s2}$ , and Laplacian matrix  $\mathcal{L}_{s2}$  are defined as follows:  $\mathcal{A}_{s2} = [0, 1, 0, 1, 0, 0; 1, 0, 1, 0, 0, 0; 0, 1, 0, 1, 0, 0; 1, 0, 1, 0, 1, 0; 0, 0, 0, 1, 0, 1; 0, 0, 1, 0, 1, 0]$ ,  $\mathcal{D}_{s2} = \text{diag}(2, 2, 2, 3, 2, 1)$ ,  $\mathcal{B}_{s2} = \text{diag}(1, 0, 0, 0, 0, 0)$ , and  $\mathcal{L}_{s2} = \mathcal{D}_{s2} - \mathcal{A}_{s2}$ .

The equation of the geometric center  $\mathcal{Q}_d$  is defined as

$$\begin{aligned} x_d &= r_d \cos 0.2\pi t + 2, \\ y_d &= r_d \sin 0.4\pi t + 3, \\ z_d &= \sin 0.4\pi t + 2 \end{aligned} \quad (51)$$

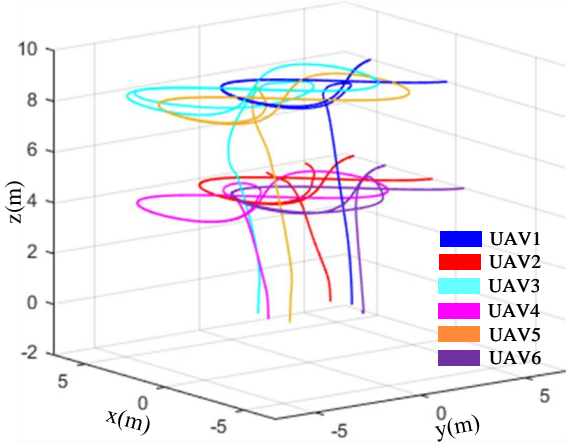


Fig. 12. Graphic demonstration of the quadrotor formation in a 3D view.

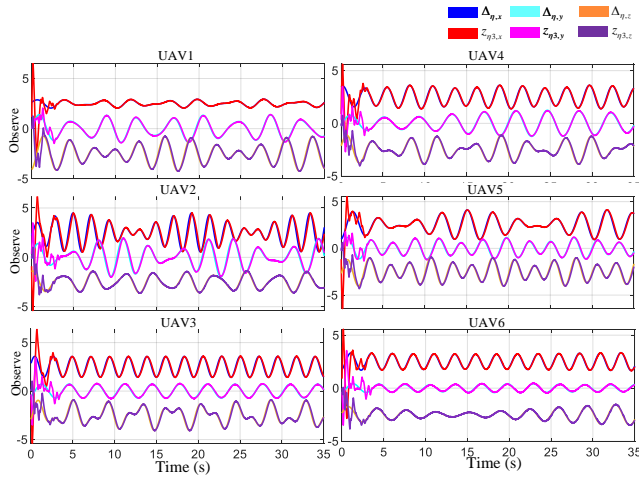


Fig. 13. Output of the observers.

with  $r_d = 5m$ . The offsets of each quadrotor to  $\mathcal{O}_d$ , denoted by  $\nu_i, i = 1, 2, \dots, 6$ , are defined as

$$\begin{aligned} \nu_1 &= [r_\nu, 0, 0]^\top, \\ \nu_2 &= [r_\nu \sin \theta_0, r_\nu \cos \theta_0, 0]^\top, \\ \nu_3 &= [-r_\nu \sin \theta_0, r_\nu \cos \theta_0, 0]^\top, \\ \nu_4 &= [-r_\nu, 0, 0]^\top, \\ \nu_5 &= [-r_\nu \sin \theta_0, -r_\nu \cos \theta_0, 0]^\top, \\ \nu_6 &= [r_\nu \sin \theta_0, -r_\nu \cos \theta_0, 0]^\top, \end{aligned} \quad (52)$$

where  $\theta_0 = 60^\circ$  and  $r_\nu = 2m$ .

Fig. 11 illustrates the 2-norm of the tracking errors across different control frameworks. Correspondingly, the three-dimensional position response of the quadrotor group is presented in Fig. 12, while the output of the FTDOs is recorded in Fig. 13. Similarly, in Figs. 7 and 11, the control performances of FNTSMC+RL" (the cyan curves) and FNTSMC+FTDO" (the red curves) are slightly better than that of the traditional FNTSMC (the blue curves), although the errors remain relatively large. In contrast, the tracking error converges rapidly to zero under the control of the FNTSMC+RL+FTDO" framework for both the double-circle" and " $\infty$ -shaped" reference

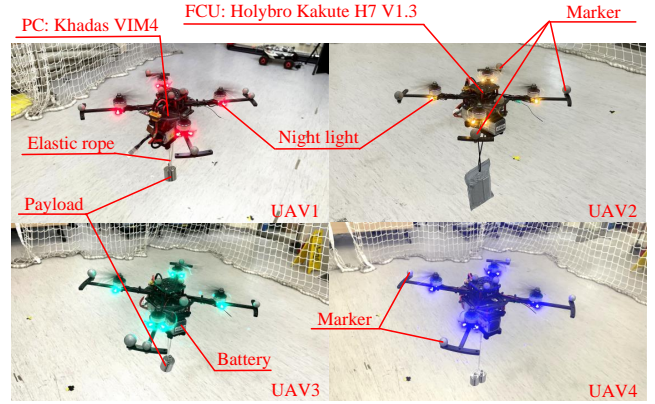


Fig. 14. The quadrotors used in the experiment.

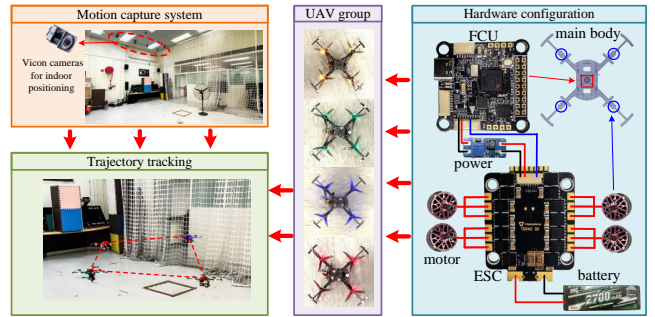


Fig. 15. The entire experiment configuration.

trajectories. Additionally, the tracking accuracy of the proposed FNTSMC-RL-FTDO framework surpasses that of the methods proposed in [26] and [42].

## VI. PHYSICAL EXPERIMENTS

This section presents real-world experiments for further validation. The quadrotors used in the experiment are depicted in Fig. 14. Each quadrotor has a mass of 0.722kg and a wheelbase of 250mm. We utilize four quadrotors to demonstrate the consensus formation control. To highlight the robustness of our proposed control method under strong disturbances, we introduce two types of disturbances in the experimental environment: high-speed rotating fans and weights suspended by elastic ropes. Additionally, the aerodynamic interactions between different aircraft in the flight formation, along with discrepancies between the UAV's center of mass and its centroid, further complicate quadrotor flight control.

The complete hardware configuration for the experiment is illustrated in Fig. 15. In this figure, four self-designed quadrotors, each featuring different night light colors, are used to form the quadrotor formation. The flight control unit (FCU) of the quadrotors is the Holybro Kakute H7 v1.3, which inherits the open-source PX4-Autopilot firmware. The on-board computer is a LattePanda Alpha 864s running Ubuntu 20.04 and ROS Noetic. The FCU is connected to the on-board computer via a USB to TTL module and utilizes the MAVROS communication protocol for real-time data transmission. The quadrotors are localized by a VICON indoor positioning system equipped with 14 high-resolution optical cameras,

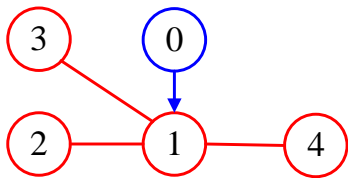
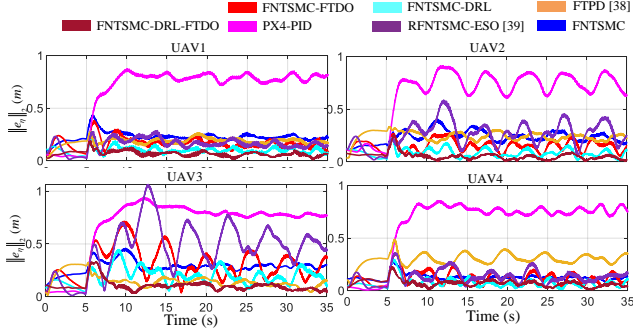


Fig. 16. Topological graph in Experiment Group 1.

Fig. 17.  $\|e_\eta\|_2$  of each quadrotor under different control frameworks.

which provide precise position and attitude feedback to the quadrotors at a frequency exceeding 200Hz. Velocity feedback is obtained by fusing data from the VICON system and the IMU using a Kalman filter. The ground station computer is used solely to monitor the states of the quadrotors and collect necessary data after the experiments. Furthermore, the ground station computer does not send any control-related commands to the quadrotor formation, as the control protocol proposed in this paper is fully distributed and decentralized.

#### A. Experiment Group 1

The topological graph of the quadrotor group is shown in Fig. 16. The adjacent matrix  $\mathcal{A}_{p1}$ , in-degree matrix  $\mathcal{D}_{p1}$ , communication matrix  $\mathcal{B}_{p1}$ , and Laplacian matrix  $\mathcal{L}_{p1}$  are respectively defined as  $\mathcal{A}_{p1} = [0, 1, 1, 1; 1, 0, 0, 0; 1, 0, 0, 0; 1, 0, 0, 0]$ ,  $\mathcal{D}_{p1} = \text{diag}(3, 1, 1, 1)$ ,  $\mathcal{B}_{p1} = \text{diag}(1, 0, 0, 0)$ , and  $\mathcal{L}_{p1} = \mathcal{D}_{p1} - \mathcal{B}_{p1}$ . The geometric center  $\mathcal{O}_d = [0, 0.2, 1.5]^\top$  remains unchanged. The offsets of each quadrotor to  $\mathcal{O}_d$ , denoted by  $\nu_i, i = 1, 2, 3, 4$ , are defined as

$$\begin{aligned}\nu_1 &= [1.3 \cos 0.4\pi t, 1.3 \sin 0.4\pi t, 0.3 \sin 0.2\pi t + 0.5]^\top \\ \nu_2 &= [-1.3 \sin 0.4\pi t, 1.3 \cos 0.4\pi t, -0.5]^\top \\ \nu_3 &= [-1.3 \cos 0.4\pi t, -1.3 \sin 0.4\pi t, 0.3 \sin 0.2\pi t + 0.5]^\top \\ \nu_4 &= [1.3 \sin 0.4\pi t, -1.3 \cos 0.4\pi t, -0.5]^\top.\end{aligned}$$

Fig. 17 illustrates the 2-norm of the consensus tracking errors under different control frameworks, while the position response in a 3D view is depicted in Fig. 18. Additionally, Fig. 17 highlights the differences in control performance across various frameworks.

Firstly, the response curve of the PID controller is notably smooth; however, it exhibits relatively large steady-state errors and phase delays. Secondly, the performance of the FNTSMC-DRL-FTDO method surpasses that of all other controllers, including those introduced in [26] and [42]. With enhancements

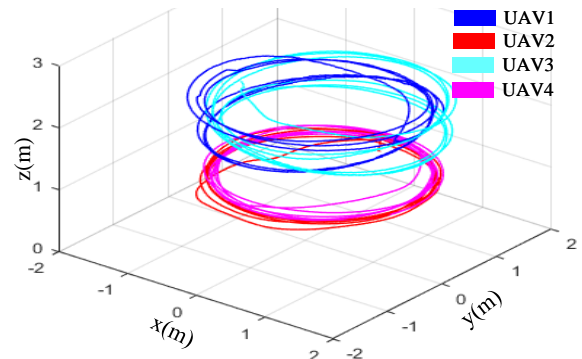


Fig. 18. Graphic demonstration of the quadrotor formation in a 3D view.

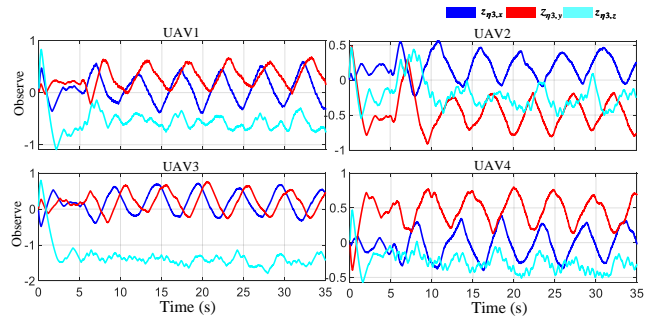


Fig. 19. Output of the observers.

in the FTDO and the DRL parameter optimizer, the proposed method stands out for its superior control performance under strong disturbances and uncertainties.

Fig. 19 illustrates the corresponding output of the FTDO. As shown in the figure, the observed outputs in the  $x$  and  $y$  directions exhibit noticeable fluctuations, with the oscillation period closely matching that of the reference trajectory for the quadrotor formation. This periodic behavior is attributed to the influence of the fans, which act as an external disturbance on the quadrotors. Additionally, the FTDO output in the  $z$  direction corresponds to an equivalent weight that closely matches the weight of the masses suspended below the quadrotor, demonstrating the effectiveness of the FTDO.

#### B. Experiment Group 2

Furthermore, we employed a more aggressive reference trajectory to test the performance of the quadrotor formation under more extreme environmental conditions. The topological graph of the quadrotor group is shown in Fig. 20. The adjacent matrix  $\mathcal{A}_{p2}$ , in-degree matrix  $\mathcal{D}_{p2}$ , communication matrix  $\mathcal{B}_{p2}$ , and Laplacian matrix  $\mathcal{L}_{p2}$  are respectively defined as  $\mathcal{A}_{p2} = [0, 1, 0, 1; 1, 0, 1, 0; 0, 1, 0, 0; 1, 0, 0, 0]$ ,  $\mathcal{D}_{p2} = \text{diag}(2, 2, 1, 1)$ ,  $\mathcal{B}_{p2} = \text{diag}(1, 0, 0, 0)$ , and  $\mathcal{L}_{p2} = \mathcal{D}_{p2} - \mathcal{B}_{p2}$ . The equation for the geometric center  $\mathcal{O}_d$  is defined as

$$x_d = \cos 0.4\pi t, \quad y_d = \sin 0.8\pi t + 0.2, \quad z_d = 1.5. \quad (53)$$

**TABLE II**  
TRACKING ERRORS OF THE QUADROTOR GROUP UNDER TWO GROUPS OF EXPERIMENTS.

Experiment Group1						
	FNTSMC	FNTSMC-FTDO	FNTSMC-RL	PX4-PID	[38]	[39]
$\sum_{i=1}^4 \ e_{\eta,i}\ _2$	210.8893	202.3448	120.8247	613.5627	226.4347	261.9122
$\sum_{i=1}^4 \ e_{\eta,i}\ _1 (\times 10^4)$	1.1409	0.9841	0.5905	3.0267	1.1450	1.2361
Experiment Group2						
	FNTSMC	FNTSMC-FTDO	FNTSMC-RL	PX4-PID	[38]	[39]
$\sum_{i=1}^4 \ e_{\eta,i}\ _2$	224.7086	134.0974	130.7996	274.9714	263.8589	124.6594
$\sum_{i=1}^4 \ e_{\eta,i}\ _1 (\times 10^4)$	0.9820	0.5438	0.5319	1.1355	1.0839	0.4707

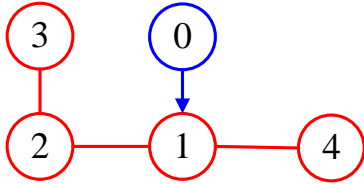
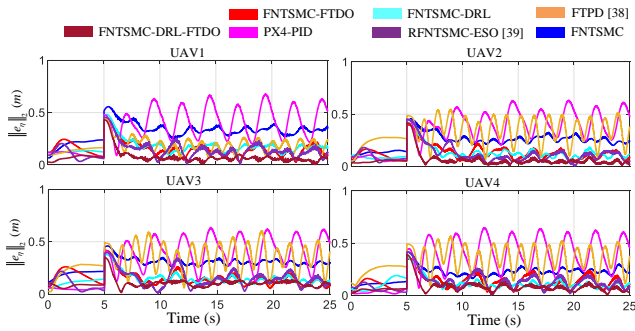


Fig. 20. Topological graph in Experiment Group 2.

Fig. 21.  $\|e_{\eta,i}\|_2$  of each quadrotor under different control frameworks.

The offsets of each quadrotor to  $\mathcal{O}_d$ , denoted by  $\nu_i, i = 1, 2, 3, 4$ , are defined as

$$\begin{aligned}\nu_1 &= [0.5, 0, 0.3 \sin 0.2\pi t + 0.5]^\top, \\ \nu_2 &= [0, 0.8, -0.5]^\top, \\ \nu_3 &= [-0.5, 0, 0.3 \sin 0.2\pi t + 0.5]^\top, \\ \nu_4 &= [0, -0.8, -0.5]^\top.\end{aligned}$$

Similarly, the 2-norm of the tracking errors, the position response in a 3D view, and the corresponding output of the FTDO are recorded in Fig. 21, Fig. 22, and Fig. 23, respectively. The error statistical curves from Experiment 2 exhibit the same pattern as those from Experiment 1, indicating that the proposed control framework consistently outperforms other methods. Specifically, we calculated the sum of the  $L_2$  and  $L_1$  norms of the consensus errors for the quadrotor formation, as presented in Table II, which clearly demonstrates the superiority of the FNTSMC-DRL-FTDO method. Finally, as shown in Fig. 23, the oscillation frequency of the observer output curve in the  $y$  direction is approximately twice that of the  $x$  direction, which aligns perfectly with the characteristics of the pre-defined reference trajectory.

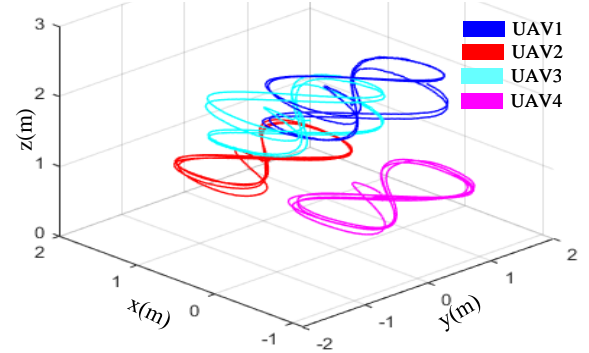


Fig. 22. Graphic demonstration of the quadrotor formation in a 3D view.

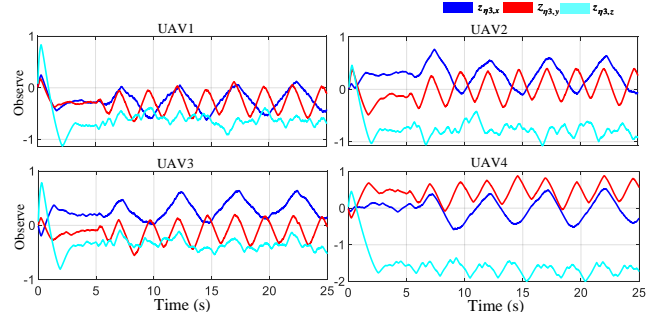


Fig. 23. Output of the observers.

## VII. CONCLUSION

This paper presents a novel robust control framework for quadrotor groups that integrates Fast Nonsingular Terminal Sliding Mode Control (FNTSMC), Deep Reinforcement Learning (DRL) techniques, and Fixed-Time Disturbance Observers (FTDO). Initially, FNTSMCs are designed for the closed-loop system. Next, FTDOs are employed to accurately estimate the uncertainties and disturbances affecting the quadrotors in fixed time. The outputs of the observers are integrated into the switching control laws of the system, thereby enhancing the robustness of the controller and improving overall control performance. The fixed-time stability of the multi-agent system is guaranteed in a Lyapunov sense. To further enhance control performance, DRL is utilized to train a parameter optimizer that adaptively tunes certain hyperparameters in the FNTSMCs based on the tracking errors of the quadrotors. Finally, extensive simulations and physical experiments are conducted to validate the effectiveness and

robustness of the proposed control framework.

## REFERENCES

- [1] E. Baccour, A. Erbad, A. Mohamed, M. Hamdi, and M. Guizani, “Multi-agent reinforcement learning for privacy-aware distributed cnn in heterogeneous iot surveillance systems,” *J. Network Comput. Appl.*, vol. 230, p. 103933, 2024.
- [2] S. Al-Hussaini, J. M. Gregory, and S. K. Gupta, “Generating task reallocation suggestions to handle contingencies in human-supervised multi-robot missions,” *IEEE Trans. Autom. Sci. Eng.*, vol. 21, no. 1, pp. 367–381, 2023.
- [3] T. Li, C. Wang, M. Q.-H. Meng, and C. W. de Silva, “Attention-driven active sensing with hybrid neural network for environmental field mapping,” *IEEE Trans. Autom. Sci. Eng.*, vol. 19, no. 3, pp. 2135–2152, 2021.
- [4] Z. Pei, T. Fang, K. Weng, and W. Yi, “Urban on-demand delivery via autonomous aerial mobility: Formulation and exact algorithm,” *IEEE Trans. Autom. Sci. Eng.*, vol. 20, no. 3, pp. 1675–1689, 2022.
- [5] J. Huang, W. Wang, C. Wen, J. Zhou, and G. Li, “Distributed adaptive leader-follower and leaderless consensus control of a class of strict-feedback nonlinear systems: A unified approach,” *Autom.*, vol. 118, p. 109021, 2020.
- [6] Z. Shang, Y. Jiang, B. Niu, G. Zong, X. Zhao, and H. Li, “Adaptive finite-time consensus tracking control for nonlinear multi-agent systems: An improved tan-type nonlinear mapping function method,” *IEEE Trans. Autom. Sci. Eng.*, vol. 21, no. 4, pp. 5434–5444, 2024.
- [7] L. Gu, Z. Zhao, J. Sun, and Z. Wang, “Finite-time leader-follower consensus control of multiagent systems with mismatched disturbances,” *Asian J. Control*, vol. 24, no. 2, pp. 722–731, 2022.
- [8] H. Zhao, L. Peng, L. Xie, and H. Yu, “Dynamic event-triggered sliding-mode bipartite consensus for multi-agent systems with unknown dynamics,” *IEEE Trans. Autom. Sci. Eng.*, pp. 1–11, 2024.
- [9] M. Khodaverdian, S. Hajshirmohamadi, A. Hakobyan, and S. Ijaz, “Predictor-based constrained fixed-time sliding mode control of multi-uav formation flight,” *Aerospace Sci. Technol.*, vol. 148, p. 109113, 2024.
- [10] Q. Miao, K. Zhang, and B. Jiang, “Fixed-time collision-free fault-tolerant formation control of multi-uavs under actuator faults,” *IEEE Trans. Cybern.*, 2024.
- [11] J. Liang, Y. Wang, H. Zhong, Y. Chen, H. Li, H. Hua, and W. Wang, “Robust adaptive tracking control for aerial transporting a cable-suspended payload using backstepping sliding mode techniques,” *IEEE Trans. Autom. Sci. Eng.*, pp. 1–11, 2024.
- [12] Y. Hou, D. Chen, and S. Yang, “Adaptive robust trajectory tracking controller for a quadrotor uav with uncertain environment parameters based on backstepping sliding mode method,” *IEEE Trans. Autom. Sci. Eng.*, pp. 1–11, 2023.
- [13] J. Liang, Y. Chen, Y. Wu, Z. Miao, H. Zhang, and Y. Wang, “Adaptive prescribed performance control of unmanned aerial manipulator with disturbances,” *IEEE Trans. Autom. Sci. Eng.*, vol. 20, no. 3, pp. 1804–1814, 2023.
- [14] S. Ijaz, M. Galea, M. T. Hamayun, H. Ijaz, and U. Javaid, “A new output integral sliding mode fault-tolerant control and fault estimation scheme for uncertain systems,” *IEEE Trans. Autom. Sci. Eng.*, vol. 21, no. 3, pp. 4214–4225, 2024.
- [15] J. Li, L. Yuan, T. Chai, and F. L. Lewis, “Consensus of nonlinear multiagent systems with uncertainties using reinforcement learning based sliding mode control,” *IEEE Trans. Circuits Syst. I Regul. Pap.*, vol. 70, no. 1, pp. 424–434, 2022.
- [16] A. Mousavi, A. H. Markazi, and E. Khanmirza, “Adaptive fuzzy sliding-mode consensus control of nonlinear under-actuated agents in a near-optimal reinforcement learning framework,” *J. Franklin Inst.*, vol. 359, no. 10, pp. 4804–4841, 2022.
- [17] J. Jia, K. Guo, X. Yu, W. Zhao, and L. Guo, “Accurate high-maneuvering trajectory tracking for quadrotors: a drag utilization method,” *Mech. Syst. Signal Process.*, vol. 7, no. 3, pp. 6966–6973, 2022.
- [18] B. Wang, X. Yu, L. Mu, and Y. Zhang, “Disturbance observer-based adaptive fault-tolerant control for a quadrotor helicopter subject to parametric uncertainties and external disturbances,” *Mech. Syst. Signal Process.*, vol. 120, pp. 727–743, 2019.
- [19] G. Wen and B. Li, “Optimized leader-follower consensus control using reinforcement learning for a class of second-order nonlinear multiagent systems,” *IEEE Trans. Syst. Man Cybern.: Syst.*, vol. 52, no. 9, pp. 5546–5555, 2021.
- [20] L. Chen, C. Dong, and S.-L. Dai, “Adaptive optimal consensus control of multiagent systems with unknown dynamics and disturbances via reinforcement learning,” *IEEE Trans. Artif. Intell.*, 2023.
- [21] S. Wang, X. Jin, S. Mao, A. V. Vasilakos, and Y. Tang, “Model-free event-triggered optimal consensus control of multiple euler-lagrange systems via reinforcement learning,” *IEEE Trans. Network Sci. Eng.*, vol. 8, no. 1, pp. 246–258, 2020.
- [22] X. Yang, H. Zhang, and Z. Wang, “Data-based optimal consensus control for multiagent systems with policy gradient reinforcement learning,” *IEEE Trans. Neural Networks Learn. Syst.*, vol. 33, no. 8, pp. 3872–3883, 2021.
- [23] Z. Hou and I. Fantoni, “Interactive leader-follower consensus of multiple quadrotors based on composite nonlinear feedback control,” *IEEE Trans. Control Syst. Technol.*, vol. 26, no. 5, pp. 1732–1743, 2017.
- [24] T. Yan, Z. Xu, and S. X. Yang, “Consensus formation tracking for multiple uav systems using distributed bioinspired sliding mode control,” *IEEE Trans. Intell. Veh.*, vol. 8, no. 2, pp. 1081–1092, 2022.
- [25] K. Liu, R. Wang, X. Wang, and X. Wang, “Anti-saturation adaptive finite-time neural network based fault-tolerant tracking control for a quadrotor uav with external disturbances,” *Aerospace Sci. Technol.*, vol. 115, p. 106790, 2021.
- [26] L. Chen, Z. Liu, Q. Dang, W. Zhao, and G. Wang, “Robust trajectory tracking control for a quadrotor using recursive sliding mode control and nonlinear extended state observer,” *Aerospace Sci. Technol.*, vol. 128, p. 107749, 2022.
- [27] Y. Hong, J. Hu, and L. Gao, “Tracking control for multi-agent consensus with an active leader and variable topology,” *Autom.*, vol. 42, no. 7, pp. 1177–1182, 2006.
- [28] Z. Zuo, B. Tian, M. Defoort, and Z. Ding, “Fixed-time consensus tracking for multiagent systems with high-order integrator dynamics,” *IEEE Trans. Autom. Control*, vol. 63, no. 2, pp. 563–570, 2017.
- [29] C. Qian and W. Lin, “A continuous feedback approach to global strong stabilization of nonlinear systems,” *IEEE Trans. Autom. Control*, vol. 46, no. 7, pp. 1061–1079, 2001.
- [30] B. Jiang, Q. Hu, and M. I. Friswell, “Fixed-time attitude control for rigid spacecraft with actuator saturation and faults,” *IEEE Trans. Control Syst. Technol.*, vol. 24, no. 5, pp. 1892–1898, 2016.
- [31] Z. Hou, P. Lu, and Z. Tu, “Nonsingular terminal sliding mode control for a quadrotor uav with a total rotor failure,” *Aerospace Sci. Technol.*, vol. 98, p. 105716, Mar. 2020.
- [32] L.-X. Xu, H.-J. Ma, D. Guo, A.-H. Xie, and D.-L. Song, “Backstepping sliding-mode and cascade active disturbance rejection control for a quadrotor uav,” *IEEE/ASME Trans. Mechatron.*, vol. 25, no. 6, pp. 2743–2753, 2020.
- [33] B. Li, W. Gong, Y. Yang, and B. Xiao, “Distributed fixed-time leader-following formation control for multiquadrotors with prescribed performance and collision avoidance,” *IEEE Trans. Aerosp. Electron. Syst.*, vol. 59, no. 5, pp. 7281–7294, 2023.
- [34] L. Zhang, Y. Xia, G. Shen, and B. Cui, “Fixed-time attitude tracking control for spacecraft based on a fixed-time extended state observer,” *Sci. China Inf. Sci.*, vol. 64, no. 11, p. 212201, 2021.
- [35] M. T. Angulo, J. A. Moreno, and L. Fridman, “Robust exact uniformly convergent arbitrary order differentiator,” *Autom.*, vol. 49, no. 8, pp. 2489–2495, 2013.
- [36] J. Schulman, F. Wolski, P. Dhariwal, A. Radford, and O. Klimov, “Proximal policy optimization algorithms,” *arXiv preprint arXiv:1707.06347*, 2017.
- [37] R. S. Sutton, D. McAllester, S. Singh, and Y. Mansour, “Policy gradient methods for reinforcement learning with function approximation,” *Adv. Neural Inf. Process. Syst.*, vol. 12, 1999.
- [38] S. M. Kakade, “A natural policy gradient,” *Adv. Neural Inf. Process. Syst.*, vol. 14, 2001.
- [39] S. Kakade and J. Langford, “Approximately optimal approximate reinforcement learning,” in *Proceedings of the Nineteenth International Conference on Machine Learning*, 2002, pp. 267–274.
- [40] J. Schulman, P. Moritz, S. Levine, M. Jordan, and P. Abbeel, “High-dimensional continuous control using generalized advantage estimation,” *arXiv preprint arXiv:1506.02438*, 2015.
- [41] T. Huang, Y. Liang, X. Ban, J. Zhang, and X. Huang, “The control of magnetic levitation system based on improved q-network,” in *2019 IEEE Symposium Series on Computational Intelligence (SSCI)*, 2019, pp. 191–197.
- [42] H. Wang, J. Shan, and H. Alkomy, “Fully distributed edge-based dynamic event-triggered control for multiple quadrotors,” *IEEE/ASME Trans. Mechatron.*, 2024.